Stem Cell Reports
Article

ISSCR

OPEN ACCESS

The AMPK/p27^{Kip1} Axis Regulates Autophagy/Apoptosis Decisions in Aged Skeletal Muscle Stem Cells

James P. White,[1,2,3,*] Andrew N. Billin,[6,7] Milton E. Campbell,[2] Alan J. Russell,[6,8] Kim M. Huffman,[2,3,4] and William E. Kraus[2,3,5]

[1]Division of Hematology, Department of Medicine, Duke University School of Medicine, Durham, NC 27710, USA
[2]Duke Molecular Physiology Institute, Duke University School of Medicine, Durham, NC 27701, USA
[3]Duke Center for the Study of Aging and Human Development, Duke University School of Medicine, Durham, NC 27701, USA
[4]Division of Rheumatology, Duke University School of Medicine, Durham, NC 27701, USA
[5]Division of Cardiology, Duke University School of Medicine, Durham, NC 27701, USA
[6]Muscle Metabolism Discovery Performance Unit, Metabolic Pathways and Cardiovascular Therapeutic Area, GlaxoSmithKline, King of Prussia, PA 19406, USA
[7]Present address: Gilead Sciences, Inc. Foster City, CA 94404, USA
[8]Present address: Edgewise Therapeutics, Boulder, CO 80303, USA
*Correspondence: james.white@duke.edu
https://doi.org/10.1016/j.stemcr.2018.06.014

SUMMARY

Skeletal muscle stem cell (MuSC) function declines with age and contributes to impaired muscle regeneration in older individuals. Acting through AMPK/p27^{Kip1}, we have identified a pathway regulating the balance between autophagy, apoptosis, and senescence in aged MuSCs. While p27^{Kip1} is implicated in MuSC aging, its precise role and molecular mechanism have not been elucidated. Age-related MuSC dysfunction was associated with reduced autophagy, increased apoptosis, and hypophosphorylation of AMPK and its downstream target p27^{Kip1}. AMPK activation or ectopic expression of a phosphomimetic p27^{Kip1} mutant was sufficient to suppress *in vitro* apoptosis, increase proliferation, and improve *in vivo* transplantation efficiency of aged MuSCs. Moreover, activation of the AMPK/p27^{Kip1} pathway reduced markers of cell senescence in aged cells, which was, in part, dependent on p27^{Kip1} phosphorylation. Thus, the AMPK/p27^{Kip1} pathway likely regulates the autophagy/apoptosis balance in aged MuSCs and may be a potential target for improving muscle regeneration in older individuals.

INTRODUCTION

Muscle stem cells (MuSCs) play a vital role in skeletal muscle regeneration (Fry et al., 2014; Moss and Leblond, 1971; von Maltzahn et al., 2013). MuSCs become dysfunctional with advanced age, leading to the inability to successfully regenerate muscle tissue after injury (Blau et al., 2015; Garcia-Prat et al., 2016b; Merlini et al., 2015). Age-associated reductions in MuSC numbers are associated with impairments in muscle regenerative capacity (Brooks et al., 2009; Collins et al., 2007; Conboy et al., 2010; Hikida, 2011; Jang et al., 2011; Shefer et al., 2010). In addition to reductions in satellite cell numbers, age-related impairments in MuSC activation contribute to sarcopenia (Sousa-Victor and Munoz-Canoves, 2016). The contribution of both systemic (Conboy et al., 2005; Sinha et al., 2014) and intracellular (Chakkalakal et al., 2012) factors influence this process; however, the mechanism(s) mediating this phenomenon are currently unclear.

Aged mammalian MuSCs have alterations in intracellular processes including autophagy and apoptosis (Garcia-Prat et al., 2016a; Jejurikar et al., 2006; Krajnak et al., 2006). Autophagy is initiated during periods of negative energy stress and generates substrates for energy production via degradation of cellular organelles and proteins (Mizushima et al., 2004). In the MuSC, autophagy provides initial energetics necessary for proliferation (Tang and Rando, 2014). Inhibition of the autophagy program results in perturbations in MuSC function including alterations in mitochondrial function, ATP production and induction of senescence (Garcia-Prat et al., 2016a; Tang and Rando, 2014). As a result, whole muscle regeneration is compromised when autophagy is genetically reduced in the MuSC (Garcia-Prat et al., 2016a). Aging MuSCs have an inherent reduction in autophagy (Garcia-Prat et al., 2016a), which contributes to the age-related dysfunction. Rescuing autophagy through genetic or pharmacological methods can recover aged MuSC function and rescue muscle regenerative capacity (Garcia-Prat et al., 2016a). Although the initial reports have established the importance of autophagy in MuSC function, upstream regulatory pathways have not been investigated, especially in the context of aging.

When autophagy is unable to meet the energy needs of activated cells, they become susceptible to apoptosis. During cell fate decisions, younger stem cells can initiate autophagy over apoptosis, while aged MuSCs are more likely to undergo apoptosis (Jejurikar et al., 2006). In an unchallenged state, *in vitro* activation of aged human MuSCs results in increased cell death (Fulle et al., 2013). Similarly, when mouse MuSCs are treated with pro-apoptotic factors such as tumor necrosis factor alpha and actinomycin D, apoptosis is more prevalent in aged MuSCs (Jejurikar

et al., 2006). Thus, aged MuSCs have alterations in both apoptosis and autophagy processes critical for muscle regenerative capacity; yet, nodal signaling pathways responsible for such perturbations are currently unknown.

The AMPK signaling pathway has emerged as a potent regulator of autophagy, apoptosis, and proliferation (Liang et al., 2007; Sanli et al., 2014; Sun et al., 2014). In times of energy stress AMPK can promote autophagy directly through phosphorylation of ULK1 (Egan et al., 2011) or indirectly through inhibition of mammalian target of rapamycin (mTOR) complex 1 by phosphorylation of the tuberous sclerosis complex 2 (Garami et al., 2003; Inoki et al., 2003a, 2003b; Tee et al., 2003; Zhang et al., 2003) and/or through phosphorylation of raptor (Gwinn et al., 2008). Furthermore, AMPK has been shown to regulate apoptosis in part, through phosphorylation of $p27^{Kip1}$ (CDKN1B) (Liang et al., 2007). In the context of the MuSC, AMPK function is necessary for optimal muscle regeneration (Fu et al., 2015; Theret et al., 2017) however, functional effects of downstream $p27^{Kip1}$ signaling in the aged MuSC warrants further investigation.

Once thought to simply function as a cyclin inhibitor, $p27^{Kip1}$ is now recognized as a critical mediator of cell fate during metabolic stress conditions. $p27^{Kip1}$ is involved in both cell-cycle inhibition and pathways related to autophagy and apoptosis (Liang et al., 2007). In times of cell stress, $p27^{Kip1}$ can prevent apoptosis by directly inhibiting Cdk2 activation and downstream activity of the pro-apoptotic factor Bax (Gil-Gomez et al., 1998; Hiromura et al., 1999). The function of $p27^{Kip1}$ is regulated by transcription (Rathbone et al., 2008), phosphorylation (Liang et al., 2002, 2007; Motti et al., 2005), degradation (Carrano et al., 1999; Montagnoli et al., 1999; Pagano et al., 1995), and subcellular location (Liang et al., 2002, 2007; Motti et al., 2005). Liang et al. (2007) reported that AMPK-dependent phosphorylation of $p27^{Kip1}$ on Thr198 promotes $p27^{Kip1}$ protein stability, resulting in more autophagy and less apoptosis. In addition, the mTOR-raptor complex can also regulate $p27^{Kip1}$ phosphorylation and cellular localization through the serum and glucocorticoid-inducible kinase (SGK) (Hong et al., 2008). In aged MuSC, there is less mRNA expression of $p27^{Kip1}$ (Chakkalakal et al., 2012), yet protein expression is greater in the nuclei where it can serve as cyclin inhibitor (Machida and Booth, 2004) with minimal effect on cell survival. In addition, $p27^{Kip1}$ expression associates with maintenance of satellite cell populations that proliferate less frequently, but have long-term self-renewal capacity (Chakkalakal et al., 2014). It follows that the functional regulation of $p27^{Kip1}$ may serve as a key regulatory pathway of both autophagy and apoptosis in MuSCs.

Here, we describe a molecular mechanism controlling apoptosis/autophagy and cell fate decisions involving AMPK signaling to the cyclin inhibitor, $p27^{Kip1}$ in MuSCs. Furthermore, our results suggest that AMPK/$p27^{Kip1}$ signaling is a critical regulatory step contributing to the phenotype of aged MuSCs.

RESULTS

Aging Leads to a Reduction in MuSC Autophagy and Increased Apoptosis

We first determined whether aging affects MuSC autophagy and apoptosis *in vitro* during the initial days (first 48 hr) in culture. To determine the temporal pattern of autophagic flux in MuSCs isolated from young mice, we measured LC3B puncta at 12, 24, and 48 hr in culture. To accumulate and quantify LC3B puncta, 12 hr prior to each time point, we treated cells with chloroquine (10 μM), an inhibitor of autophagosome and lysosomal fusion (Figure S1A). During the first 48 hr in culture, puncta increased steadily in young MuSCs: puncta were abundant after 24 hr in culture and further increased at 48 hr. We next determined MuSC autophagic flux across a time course of physiological aging after 48 hr in culture. LC3B puncta was determined in MuSCs from 3 to 4 months (young), 12 months (middle-aged), 24 months (old), and >28 months (geriatric) mice. Compared with young cells, there was no change in flux in the middle-aged group (Figure 1A). In contrast, puncta formation was less in old MuSCs and even less in geriatric cells. A parallel experiment measuring protein expression of LC3B I and II isoforms showed similar trends. We observed a reduction in both LC3B I and II isoforms in old cells and a further reduction in geriatric cells (Figure 1B). Using the same time course of murine aging, we quantified markers of apoptosis, observing an inverse relationship between autophagy and apoptosis with aging. Protein expression of a marker of apoptosis, cleaved poly(ADP-ribose) polymerase (PARP), was minimal in young and middle-aged cells; however, expression was observed in old cells and was even greater in geriatric cells (Figures 1C and S1C). We also examined apoptosis by analysis of TUNEL and Annexin V staining. Again, compared with young and middle-aged cells, old, and geriatric cells had progressively more TUNEL and Annexin (+) cells (Figures 1D and S1D). In sum, MuSCs from aging mice exhibited progressively less autophagy and increased apoptosis across the lifespan; these trends were especially apparent in the geriatric mice, a state associated with reduced MuSC proliferative capacity (Figure 1E).

Geriatric MuSCs Are Preferentially Susceptible to Cell Death during Autophagy Suppression

To determine whether there was a causal relationship between the reduction in autophagy and increase in

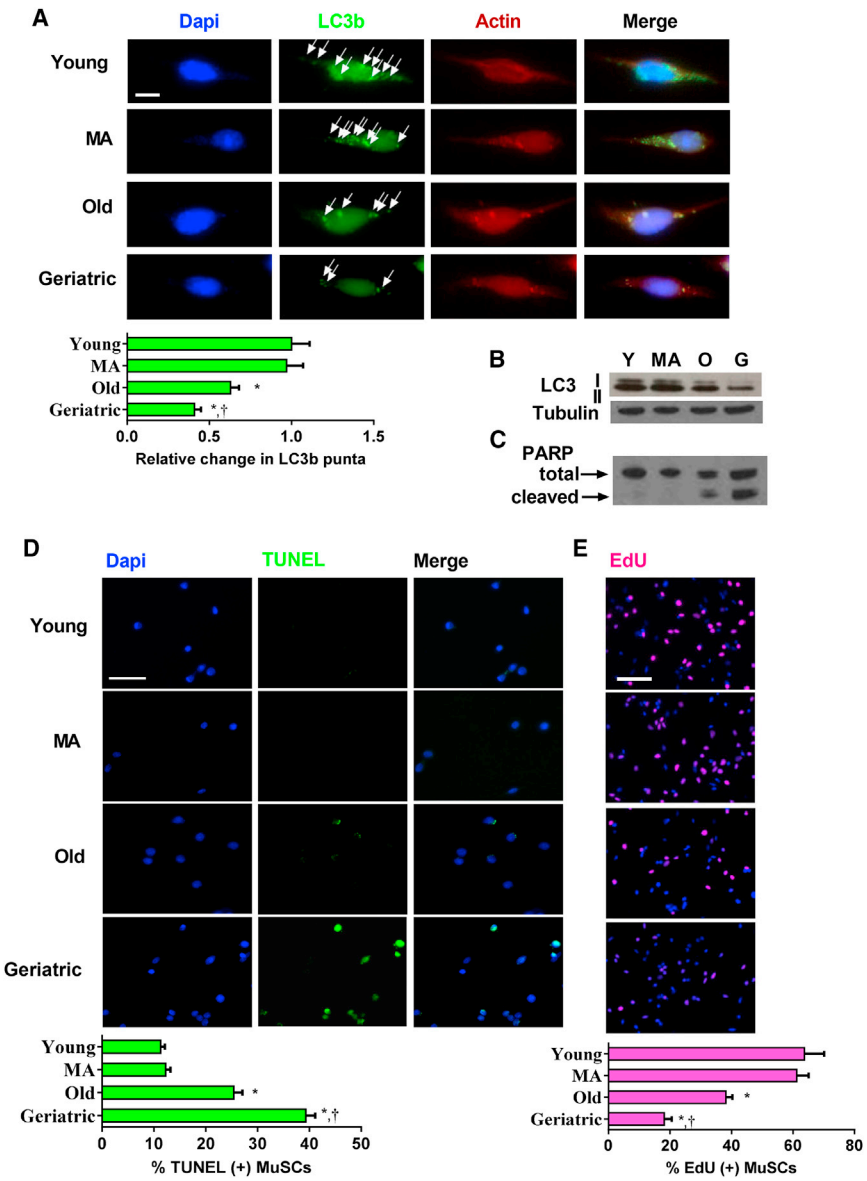

Figure 1. Altered Autophagy and Apoptosis in Aged MuSCs

MuSCs were isolated throughout a time course of aging and plated for 48 hr for autophagy and apoptosis markers.

(A) Upper: representative images of LC3B punta after 10 μM chloroquine treatment in the final 12 hr of culture. Arrowheads indicate LC3B punta. Lower: quantification of relative punta number within age groups. DAPI, blue; LC3B, green; actin, red (N = 3 independent experiments) (A). Scale bar, 5 μm. Representative western blot of LC3B isoforms I and II after 10 μM chloroquine treatment in the final 12 hr of culture (B).

(C) Total and cleaved PARP protein expression in MuSCs after 48 hr in culture.

(D) Upper: representative TUNEL staining during respective ages. DAPI, blue; TUNEL, green. Scale bar, 50 μm. Lower: quantification of percentage TUNEL-positive MuSCs (N = 4 independent experiments).

(E). Upper: representative EdU staining during respective ages. DAPI, blue; EdU, pink. Scale bar, 100 μm. Lower: quantification of percentage EdU-positive MuSCs (N = 3 independent experiments).

* Signifies different from young; † signifies different than old ($p < 0.05$). Data are presented as means ± SE.

MuSC apoptosis, we inhibited autophagy via lentivirus containing a short hairpin antisense RNA to Atg5, a key protein in formation of the autophagosome (Hara et al., 2006). The knockdown resulted in an 82% less Atg5 mRNA (Figure S2A) and 87% less Atg5 protein expression (data not shown). The reduction in Atg5 expression after 24 hr of infection resulted in a marked suppression of MuSC autophagy; this was indicated by the lack of LC3B isoform II protein expression (Figure S2B).

Suppression of autophagy did not induce apoptosis in young MuSCs (Figure 2A). In contrast, geriatric MuSCs were especially sensitive to autophagy suppression. Apoptosis increased by nearly 2-fold. Similar effects were observed with measurement of cell proliferation. The inhibition of autophagy by Atg5 knockdown delayed, but did not inhibit young MuSC proliferation throughout 72 hr in culture (Figure 2B). Geriatric MuSCs failed to undergo proliferation under these conditions (Figure 2B). To confirm the induction of apoptosis is associated with cell death, we quantified cell number for each treatment (Figure S2C). A total of 250 cells were plated for both young and geriatric groups with or without Atg5 knockdown. After 72 hr of autophagy inhibition, nearly half the geriatric cells were lost (Figure S2C). Autophagy has been linked to both canonical and non-canonical apoptotic pathways in adult stem cells (Chung and Yu, 2013). To investigate if the observed induction of cell death was through the canonical apoptotic pathways, we replicated

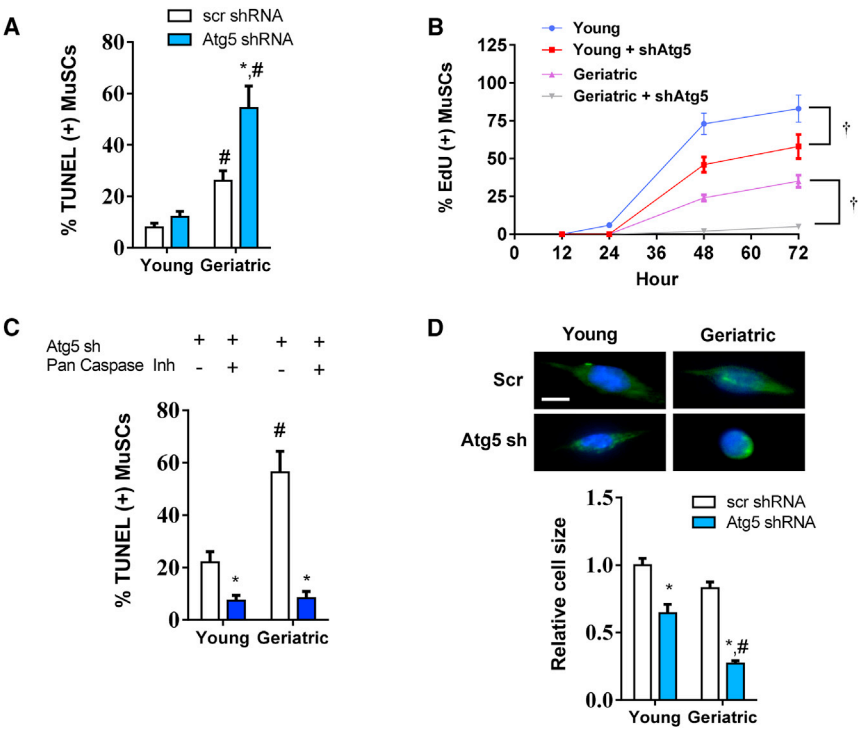

Figure 2. Aged MuSCs Are Highly Susceptible to Apoptosis during Conditions of Autophagy Impairment

(A) Percentage of TUNEL-positive cells in young and geriatric groups infected with scramble or Atg5 sh lentivirus (N = 3 independent experiments). (B) A 72-hr time course of EdU labeling in young and geriatric MuSCs with or without an sh to Atg5 (N = 3 independent experiments).

(C) Percentage of TUNEL-positive cells in young and geriatric cells infected with Atg5 sh with or without caspase inhibitor Q-VD-OPh (N = 4 independent experiments).

(D) Upper: representative images of young and geriatric MuSCs infected with GFP scramble or shAtg5 lentivirus for 48 hr in culture. Lower: quantification of relative cell size normalized to young control cells (N = 3 independent experiments). Scale bar, 5 μm. Actin, green; nuclei, blue.

* Difference among age-matched treatment groups; # different from treatment-matched young cells; † difference between age-matched groups at 48 and 72 hr ($p < 0.05$). Data are presented as means ± SE.

the Atg5 knockdown experiments in both young and geriatric cells, with or without a pan-caspase inhibitor (Figure 2C). In both young and geriatric cells, the caspase inhibitor rescued the induction of cell death caused by inhibition of autophagy. Further investigation of the canonical apoptotic pathway showed overexpressed of Bcl2 under conditions of autophagy suppression via shATG5 expression was able to attenuate the onset of apoptosis (Figure S2D). Thus, apoptosis-induction via autophagy withdrawal appears to be dependent on the canonical apoptotic pathway. In morphologic analyses, 48 hr of Atg5 knockdown modestly reduced cell size in the young MuSC. However, the surviving geriatric Atg5 knockdown MuSCs failed to hypertrophy based on quantification of cell size (Figure 2D).

Restoring AMPK Activity Prevents Cell Death in Aged MuSCs

We next sought a mechanism for the susceptibility of geriatric MuSCs to cell death under autophagy withdrawal. AMPK can regulate both autophagy and apoptosis through phosphorylation of the downstream target, $p27^{Kip1}$ (Liang et al., 2007). In young MuSCs, phosphorylation of AMPK (Thr172) and $p27^{Kip1}$ (Thr198) increased during the initial 48 hr in culture (Figure 3A). Comparing across age groups, we observed reduced AMPK/$p27^{Kip1}$ phosphorylation in old mice; this was further reduced in geriatric mice at 48 hr in culture (Figure 3B). To determine if rescue of AMPK activation would prevent cell death in geriatric MuSCs, we treated cells with the AMP analog, 5-aminoimidazole-4-carboxamide ribonucleotide (AICAR). AICAR was effective at activating AMPK in geriatric MuSCs, as indicated by phosphorylation at Thr172 and increased AMPK-specific phosphorylation of $p27^{Kip1}$ (Figure S3A). As signified by reductions in TUNEL staining (Figure 3C) and expression of cleaved PARP (Figure 3D), AICAR was sufficient to prevent cell death. To investigate the functional role of AMPK in the MuSC we genetically enhanced or suppressed AMPK activity before transplantation into injured muscle from young severe combined immunodeficiency (SCID) hosts (Figure 3E). Transplantation efficiency was high in young control MuSCs, showing numerous GFP(+) cells 4 days after transplantation (Figure 3F) and eventually incorporated into GFP(+) myofibers after 28 days (Figure 3F). Forced expression of a dominate negative AMPK prior to transplantation in young cells resulted in a roughly 70% reduction in GFP(+) donor cells/myofibers at each respective time point. Geriatric MuSCs had inherently poor transplantation efficiency, as represented by the presence of few GFP(+) cells at 4 days and GFP(+) myofibers at 28 days after transplant (Figure 3G). Prior forced expression of constitutively active AMPK to geriatric cells increased the number of GFP(+) cells and myofibers at 4 and 28 days after transplantation, respectively (Figure 3G). To show further physiological relevance to the AMPK/$p27^{Kip1}$ pathway, we isolated MuSCs from old mice with

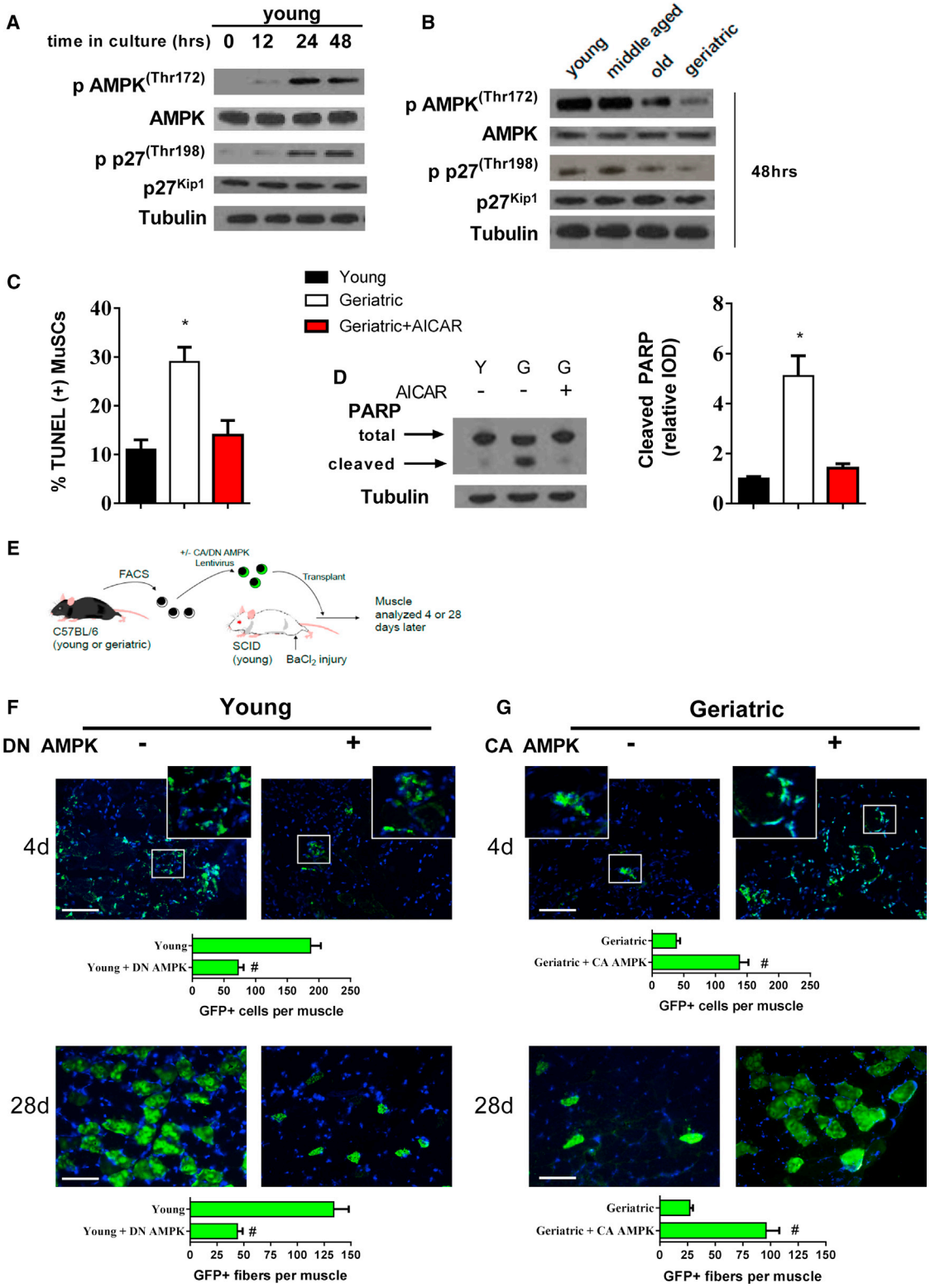

Figure 3. Restored AMPK Activation Rescues Inherent Apoptotic Susceptibility in Geriatric MuSCs

(A) Phosphorylated and total protein expression of young MuSC AMPK and $p27^{Kip1}$ throughout 48 hr in culture.

(B) Phosphorylated and total protein expression of AMPK and $p27^{Kip1}$ at 48 hr in culture across different ages.

(legend continued on next page)

or without short-term caloric restriction (CR) (40% CR), an established method to enhance MuSC function in old mice (Cerletti et al., 2012). After 48 hr in culture, phosphorylated and total forms of each protein were measured to determine if CR-mediated effects were associated with activation of the AMPK/$p27^{Kip1}$ pathway in old MuSCs. MuSCs from CR-treated old mice increased phosphorylation status of AMPK and $p27^{Kip1}$ compared with old mice fed *ad libitum* (Figure S3B).

$p27^{Kip1}$-Mediated Cell Survival Is Dependent on AMPK-Specific Thr198 Phosphorylation

After establishing the importance of AMPK signaling for regulation of cell survival and proliferation in the aging MuSC, we investigated downstream regulation of $p27^{Kip1}$ function in the MuSC. Based on previously reported constructs (Liang et al., 2007), we generated lentiviral mutants of $p27^{Kip1}$, identified as $p27^{Kip1(198A)}$ and $p27^{Kip1(198D)}$. The $p27^{Kip1(198A)}$ mutant cannot be phosphorylated at the AMPK-specific Thr 198, while $p27^{Kip1(198D)}$ serves as a Thr 198 phosphomimetic. We confirmed the potent suppression of AMPK-specific phosphorylation in the $p27^{Kip1(198A)}$ mutant after 24 hr of forced expression (Figure S4A). Next, we showed the anti-apoptotic effects of AICAR were dependent on phosphorylation of $p27^{Kip1}$. Overexpression of the $p27^{Kip1}$ mutant $p27^{Kip1(198A)}$, negated the effect of AICAR on MuSC cell death (Figure 4A) and protein expression of cleaved PARP (Figure 4B). To further validate AMPK/$p27^{Kip1}$ signaling as a cell survival mechanism, we suppressed autophagy in young and geriatric cells with concurrent overexpression of the $p27^{Kip1(198A)}$ or $p27^{Kip1(198D)}$ mutants. In the young MuSC, overexpression of the constitutively active $p27^{Kip1(198D)}$ had minimal effect on cell death; however, overexpression of $p27^{Kip1(198A)}$ resulted in increased cell death (Figure 4C). In geriatric MuSCs, overexpression of $p27^{Kip1(198D)}$ rescued the discernible induction of cell death during Atg5 knockdown, in contrast, the $p27^{Kip1(198A)}$ mutant could not rescue the induction of cell death. Overexpression of the $p27^{Kip1(198D)}$ mutant also prevented cleaved PARP expression in both untreated and ATG5 knockdown geriatric MuSCs (Figure S4B).

Next, tested whether the phosphomimetic $p27^{Kip1(198D)}$ mutant could prevent cell death without upstream AMPK activation. We treated young MuSCs with the AMPK inhibitor compound C (10 μM) for 48 hr with or without forced expression of the of $p27^{Kip1(198D)}$ mutant. Compound C was effective in suppressing AMPK phosphorylation and phosphorylation of downstream AMPK target $p27^{Kip1}$ in young MuSCs 48 hr in culture (Figure S4C). Compound C treatment nearly doubled the incidence of cell death in the young MuSC; this result was blocked by overexpression of $p27^{Kip1(198D)}$ (Figure 4D), further establishing $p27^{Kip1}$ as a pro survival mechanism. We then tested the role of AMPK/$p27^{Kip1}$ signaling in transplanted geriatric MuSCs (Figure 4E). Similar to genetic AMPK gain of function, AICAR treatment to geriatric MuSCs resulted in a high number of GFP(+) cells 4 days after transplantation (Figures 4F and 4G). The inability of AMPK to phosphorylate $p27^{Kip1}$ decreased AICAR-induced enhancement of transplantation efficiency as shown by a vast reduction in GFP(+) cells. Overexpression of the phosphomimetic $p27^{Kip1(198D)}$ was sufficient to improve transplantation capacity independent of AICAR treatment (Figures 4F and 4G). At 28 days after transplantation, AICAR pre-treatment resulted in the sustainable incorporation of geriatric MuSCs as represented by GFP(+) myofibers (Figures 4H and 4I). Concomitant overexpression of $p27^{Kip1(198A)}$ once again reduced AICAR-related effects while overexpression of $p27^{Kip1(198D)}$ showed an AICAR-independent increase in GFP(+) myofibers 28 days after transplantation (Figures 4H and 4I).

Cellular Location of $p27^{Kip1}$ Dictates Function in the Activating MuSC

The anti-apoptotic capacity of $p27^{Kip1}$ is dependent on its translocation from the nuclei to the cytoplasm (Liang et al., 2002, 2007; Wu et al., 2006). To investigate whether the same is true in activating MuSCs, we determined the localization pattern of $p27^{Kip1}$ in quiescent and activated MuSCs. Across all aging groups, $p27^{Kip1}$ was located in the nuclei in freshly isolated quiescent MuSCs (Figure 5A). After 48 hr in culture, $p27^{Kip1}$ in young MuSCs was located purely in the cytoplasm; in contrast old MuSCs had roughly equal amount in the nuclei and cytoplasm; in geriatric MuSCs

(C) TUNEL-positive cells in young, geriatric and geriatric MuSCs treated with AICAR (N = 3 independent experiments). (D). Left: representative blot of total and cleaved PARP; right: quantification of cleaved PARP protein expression normalized to young cells (N = 3 independent experiments).

(E) Young and geriatric MuSCs infected with respective AMPK lentivirus, transplanted into injured SCID muscle and quantified 4 or 28 days later. (F and G) Upper: young GFP-labeled MuSCs overexpressing GFP control or a dominant-negative (DN) AMPK 4 days; lower: 28 days after transplantation (N = 5 independent experiments) (F). Upper: geriatric GFP-labeled MuSCs overexpressing GFP control or constitutively active (CA) AMPK 4 days; lower: 28 days after transplantation. Quantification includes counts of GFP(+) cells (4d) or myofibers (28d) per muscle (N = 5 independent experiments) (G).

* Signifies difference from young cells; # signifies difference from GFP control transplanted cells ($p < 0.05$). Scale bars, 100 μm. Data are presented as means ± SE.

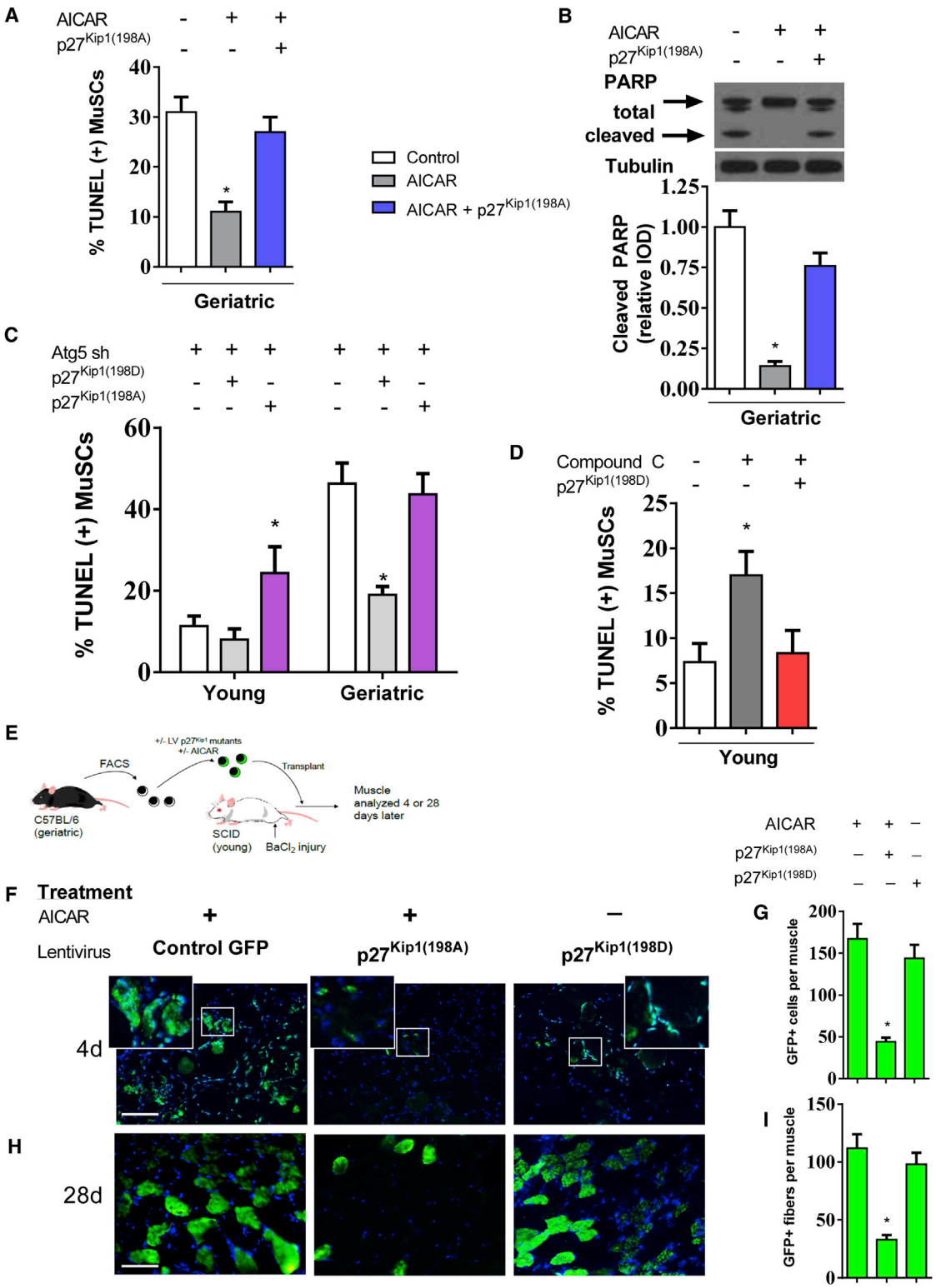

Figure 4. AMPK/p27^{Kip1} Signaling Mediates Cell Survival in the MuSC

Geriatric MuSCs were cultured for 48 hr treated with or without AICAR and/or overexpression of p27^{Kip1} mutant-p27$^{Kip1(198A)}$.

(A) Percentage of TUNEL-positive cells with respective treatment (N = 4 independent experiments).

(legend continued on next page)

p27^{Kip1} remaining primarily in nuclei (Figure 5B). We made similar observations with p27^{Kip1} staining in young and geriatric MuSCs after 48 hr in culture (Figure S5A). Furthermore, we demonstrated the efficacy of AICAR treatment in geriatric MuSCs to translocate p27^{Kip1} to the cytosol (Figure S5A). We also tested the cellular location of the p27^{Kip1} mutants. Overexpression of the p27$^{Kip1(198A)}$ mutant was located primarily in the nuclei; in contrast, the AMPK phosphomimetic p27$^{Kip1(198D)}$ mutant was located in the cytoplasm (Figure S5B).

Next, we determined if the cytoplamic p27^{Kip1} could induce autophagy as previously reported in non-muscle cell lines (Liang et al., 2007). Overexpression of the p27$^{Kip1(198D)}$ in young activated MuSCs increased LC3B puncta by roughly 50% (Figure 5C); and increased the ratio of LC3B II:I by 2-fold (Figure 5D). As indicated by immunofluorescence or protein analysis, overexpression of the p27$^{Kip1(198A)}$ mutant did not affect MuSC autophagy (Figures 5C and 5D). The ability to translocate p27^{Kip1} out of the nuclei appeared critical for cell proliferation. Young MuSCs overexpressing p27$^{Kip1(198A)}$ had a marked reduction in EdU labeling (Figure 5E). In contrast, overexpression of the p27$^{Kip1(198D)}$ mutant rescued proliferation in geriatric MuSCs. This effect was dependent on the induction of autophagy, as Atg5 knockdown negated the proliferative effects on p27$^{Kip1(198D)}$ overexpressing geriatric MuSCs (Figure 5F). These data suggest p27^{Kip1} induces cell survival in an autophagy-independent fashion, while its proliferative effects are autophagy dependent.

AMPK Activation through p27^{Kip1} Regulates Cellular Senescence

Loss of autophagy in satellite cells of young mice results in the induction of senescence markers (Garcia-Prat et al., 2016a). We sought to determine if restoring AMPK signaling activity would suppress senescence markers. Beta-galactosidase (β-gal), an established senescence marker (Dimri et al., 1995), was greater in old MuSCs and even greater in geriatric cells (Figure S6). AICAR treatment in geriatric cells suppressed β-gal staining (Figure 6A). Overexpression of the p27$^{Kip1(198A)}$ mutant attenuated AICAR-induced suppression of β-gal staining (Figure 6A). Similar effects were observed when quantifying protein expression of phosphorylated S6 Kinase (Figure 6B). mRNA expression of senescence genes p16INK4a and p21CIP1 increased in geriatric MuSCs (Figure 6C). AICAR treatment prevented p16INK4a and p21CIP1 expression while overexpression of p27$^{Kip1(198A)}$ attenuated this effect. Thus, the AMPK/p27^{Kip1} pathway appears to regulate MuSC cellular senescence in addition to the autophagy and apoptotic processes.

DISCUSSION

Stem cell transition from quiescence to cell-cycle entry is a critical transformation. As cells proceed to the "blast" phenotype, in order to facilitate energy production and morphological changes, there is cytoplasmic hypertrophy (Rodgers et al., 2014). Cellular anabolism comes with high energy demands. As these processes require energy in excess of the minimal energy stores of the activating stem cell, this is a period of relative energy deficit and nutrient stress. Until energy demands are met or adequate survival measures are in place, the cell is susceptible to apoptosis. Our data support the role of AMPK/p27^{Kip1} signaling in ensuring cell survival through prevention of apoptosis and enhancing the autophagy program during early activation (Figure 6D). Defects in this pathway, through aging or genetic manipulation, lead stem cells to default to apoptosis or senescence (Garcia-Prat et al., 2016b).

Cell fate is determined by a delicate balance between energy availability and survival mechanisms. The interplay between autophagy and apoptosis is becoming increasing apparent across many cell types (Ravanan et al., 2017). In the MuSC, autophagy is critical for activation and proliferation, acting as a temporary energy reserve to fuel the initial stages of cell proliferation (Tang and Rando, 2014). Aging MuSCs have a reduction in autophagy while

(B) Upper: representative blot of total and cleaved PARP; lower: quantification of protein expression normalized to untreated geriatric cells (N = 3 independent experiments).
(C) Percentage of TUNEL-positive cells during Atg5 knockdown with concurrent overexpression of p27^{Kip1} mutants p27$^{Kip1(198D)}$ or p27$^{Kip1(198A)}$ (N = 3 independent experiments).
(D) Percentage of TUNEL-positive cells during treatment of compound C to young MuSCs with concurrent overexpression of p27^{Kip1} mutant p27$^{Kip1(198D)}$ (N = 3 independent experiments).
(E) Geriatric MuSCs treated with or without AICAR and infected with respective p27^{Kip1} mutant lentivirus. Cells were transplanted into injured young SCID muscle and quantified 4 or 28 days later.
(F) Geriatric MuSCs treated with or without AICAR and overexpression of p27^{Kip1} mutants analyzed 4 days after transplantation.
(G) Quantification of GFP(+) cells per muscle (N = 6 independent experiments).
(H) Geriatric MuSCs treated with or without AICAR and overexpression of p27^{Kip1} mutants analyzed 28 days after transplantation.
(I) Quantification of GFP(+) myofibers per muscle (N = 6 independent experiments).
Scale bar, 100 μm. * Signifies difference from young or untreated control cells ($p < 0.05$). Data are presented as means ± SE.

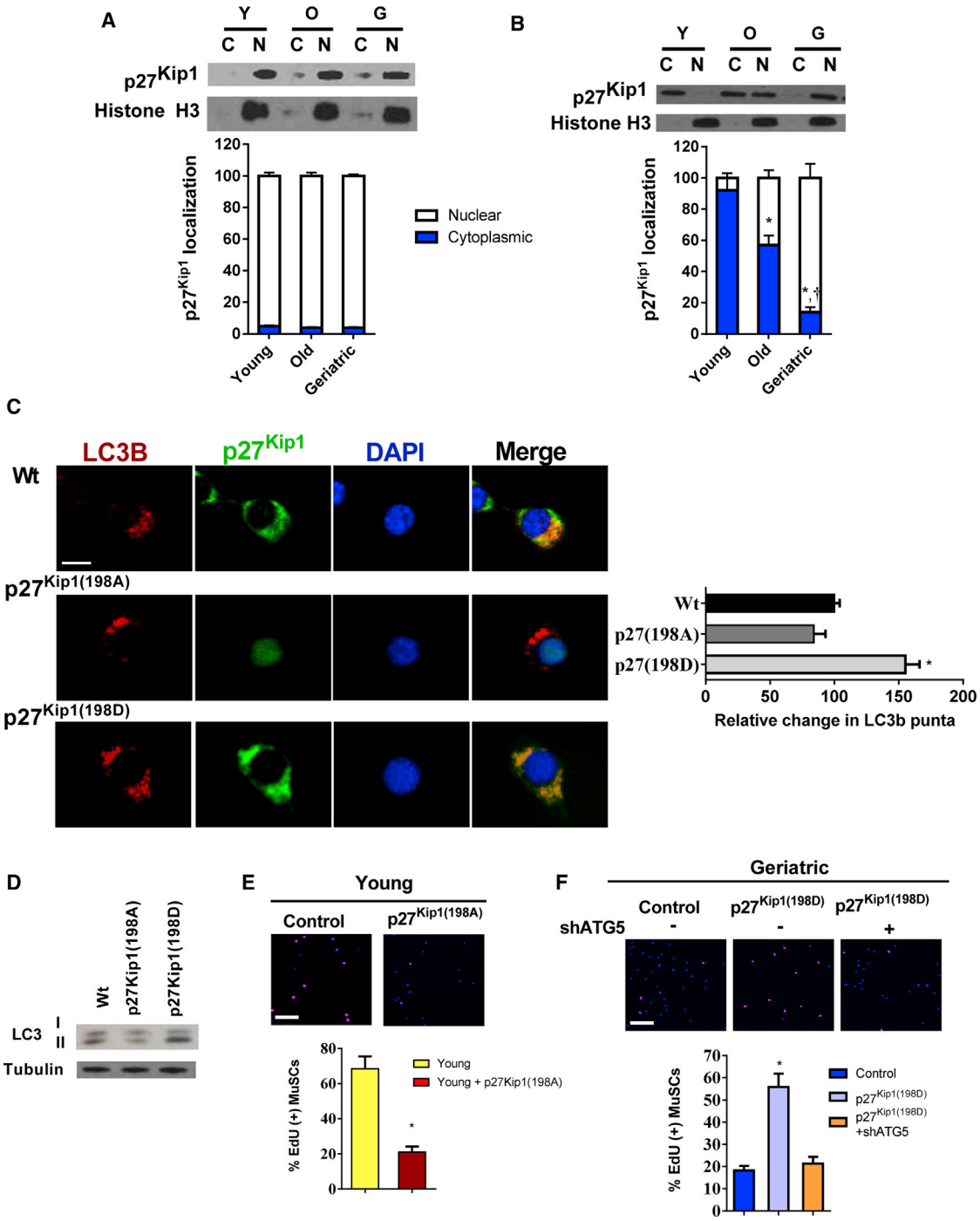

Figure 5. Cellular Location of $p27^{Kip1}$ Regulates MuSC Function in Part through the Induction of Autophagy

(A) Upper: $p27^{Kip1}$ protein expression in both cytoplasmic and nuclear compartments of freshly sorted MuSCs across age groups. Lower: quantification of percentage of cytoplasmic and nuclear expression of $p27^{Kip1}$ (N = 3 independent experiments).

(B) Upper: $p27^{Kip1}$ protein expression in both cytoplasmic and nuclear compartments of activated MuSCs (48 hr in culture) across age groups. Lower: quantification of percentage of cytoplasmic and nuclear expression of $p27^{Kip1}$ (N = 3 independent experiments).

(C) $p27^{Kip1}$ phosphorylation status-mediated cellular location and autophagy. Left: immunofluorescence staining of LC3B and $p27^{Kip1}$ expression of young MuSCs overexpressing GPF-labeled WT $p27^{Kip1}$, $p27^{Kip1(198A)}$, or $p27^{Kip1(198D)}$. All cells were treated with chloroquine for

(legend continued on next page)

rescuing the aged-related defect has a rejuvenating effect, improving function and suppressing senescence (Garcia-Prat et al., 2016a). Aged MuSCs are more susceptibility to cell death when challenged with cellular stress (Jejurikar et al., 2006). We observed an age-dependent reduction in autophagy during the initial days of *in vitro* activation, associated with reduced proliferation and increased apoptosis. Furthermore, advanced age leaves the MuSC extremely susceptible to apoptosis under conditions of autophagy suppression. This is in contrast to what happens in young MuSCs during autophagy suppression (Tang and Rando, 2014), suggesting the possible presence of age-related perturbations in key survival mechanisms.

The AMPK pathway promotes cell survival during times of nutrient stress. Although AMPK targets numerus proteins and cellular pathways (Sanli et al., 2014), downstream signaling to the multifunctional $p27^{Kip1}$ can induce autophagy; increase proliferation; and increase cell survival (Liang et al., 2007; Sun et al., 2014). We hypothesized and subsequently observed this pathway to be relevant in activating MuSCs. In activated young MuSCs, there was greater phosphorylation of AMPK and its downstream target $p27^{Kip1}$ yet, in activated old and geriatric cells, there was less phosphorylation of these proteins. This observation is consistent with the idea that aging reduces AMPK sensitivity in muscle and likely throughout all organs and tissues (Salminen and Kaarniranta, 2012). Activation of the AMPK pathway by AICAR prevented apoptosis in aged cells; conversely, AMPK inhibition in young cells resulted in greater apoptosis. The lack of AMPK signaling could explain the differential age effects of apoptosis under autophagy inhibition. In the young MuSC, AMPK activation suppresses apoptosis and results in succeeding energy production, while the aged MuSC has a reduction in AMPK activity and the added stress of suppressed autophagy defaults the cell to apoptosis.

We observed the anti-apoptotic capacity of AMPK is dependent on phosphorylation and subsequent cytoplasmic translocation of $p27^{Kip1}$. Machida and Booth (2004) reported aged MuSCs to have a greater expression of nuclear $p27^{Kip1}$; we confirmed these findings. However, our data suggest cellular location of $p27^{Kip1}$ is dynamic, shifting from the nucleus to the cytoplasm as the cell undergoes activation. Failure to translocate $p27^{Kip1}$ during activation is one mechanism of age-related cellular dysfunction. Maintaining $p27^{Kip1}$ in the nuclei not only inhibits cell-cycle progression, it also leaves the cell susceptible to apoptosis. In fact, inhibition of the cytoplasmic translocation of $p27^{Kip1}$ is a popular pharmacological target to encouraging cell death in various cancer cell line (Hiromura et al., 1999; Liang et al., 2002; Motti et al., 2005; Wu et al., 2006). Our current work shows the potency of this pathway and its dysfunction with age in the MuSC.

Our current work and that of others (Garcia-Prat et al., 2016a) show advanced age drives senescence in muscle MuSCs. Considering the potency of the AMPK/$p27^{Kip1}$ pathway in revitalizing cellular function in aged MuSCs, we strove to determine its regulatory role in senescence. AMPK activation was effective in blocking the induction of senescence markers. However, inability of AMPK to phosphorylate $p27^{Kip1}$ negated these effects. Autophagy is a negative regulator of MuSC senescence (Garcia-Prat et al., 2016a). The translocation of $p27^{Kip1}$ from the nuclei to the cytoplasm could play a role in preventing senescence by relieving the breaks on the cell cycle and promoting autophagy.

In sum, we observed a reduction in autophagy and more apoptosis in activating aged MuSCs when compared with their younger counterparts. This effect was due, in part by inactivation of the AMPK/$p27^{Kip1}$ pathway. Reactivation of AMPK and/or downstream $p27^{Kip1}$ translocation restored proliferation and cell survival in aged MuSCs. We observed functional differences in cytoplasmic and nuclear $p27^{Kip1}$, the former enhancing cell survival and autophagy and the later promoting quiescence, apoptosis, and senescence. Thus, dysfunctional signaling of the AMPK/$p27^{Kip1}$ pathway may be a central mechanism for age-induced loss of MuSCs, subsequent decline in regenerative function and perhaps a mechanism of and a viable target for enhancing regeneration in aged muscle.

EXPERIMENTAL PROCEDURES

Animals

C57BL/6J (wild-type [WT]) mice were used at 3–4, 12, 24, or >28 months of age. All aged mice were obtained from the GSK aging

the final 12 hr of culture. LC3B, red; $p27^{Kip1}$, green; DAPI, blue. Scale bar, 5 μm in (C). Right: quantification of relative change in LC3B puncta across treatment groups (N = 3 independent experiments).

(D) LC3B isoform protein expression in young MuSCs overexpressing WT $p27^{Kip1}$, $p27^{Kip1(198A)}$, or $p27^{Kip1(198D)}$.

(E) Upper: EdU incorporation in control or $p27^{Kip1(198A)}$ overexpressing young MuSCs. Lower: quantification of percentage of EdU(+) MuSCs in each group (N = 3 independent experiments).

(F) Upper: EdU incorporation in control, $p27^{Kip1(198A)}$ overexpressing or $p27^{Kip1(198D)}$ overexpressing geriatric MuSCs with or without Atg5 knockdown. Lower: quantification of percentage of EdU(+) MuSCs in each group (N = 3 independent experiments).

* Signifies difference from young or control cells; † signifies difference from old cells ($p < 0.05$). Scale bars, 100 μm in (E) and (F). Data are presented as means ± SE.

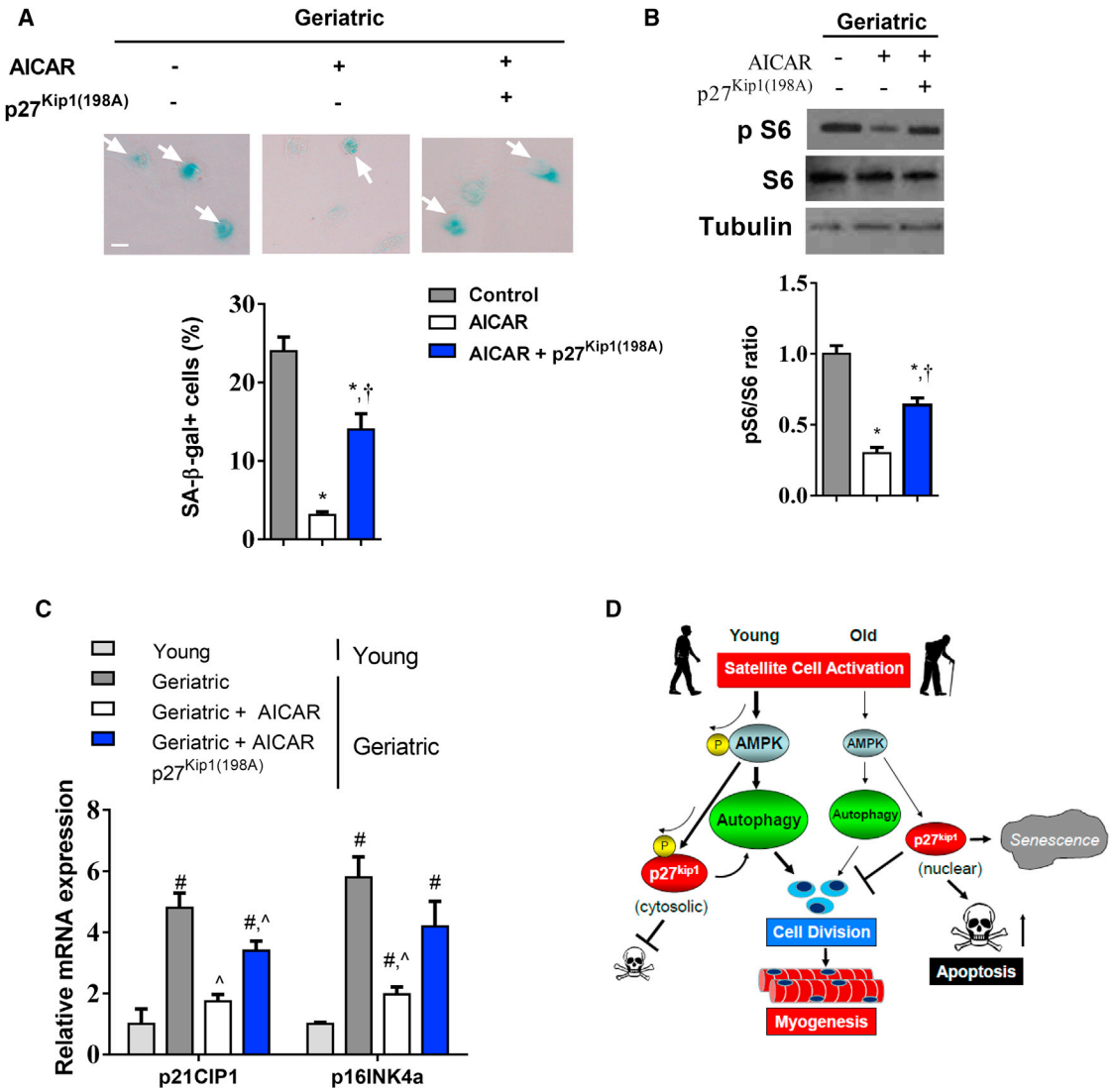

Figure 6. The AMPK/p27^{Kip1} Pathway Regulates Cellular Senescence

(A) Upper: β-gal staining in geriatric MuSCs treated with AICAR and simultaneous overexpression of p27$^{Kip1(198A)}$. Arrows represent β-gal-positive cells. Lower: percentage of β-gal-positive cells in each group (N = 3 independent experiments).

(B) Upper: representative western blot of phosphorylated and total S6 kinase protein expression. Lower: quantification of phospho/total S6 ratio normalized to geriatric control cells (N = 4 independent experiments). (C) mRNA expression of p21^{CIP1} and p16^{INK4a} in young and geriatric MuSCs treated with AICAR with or without p27$^{Kip1(198A)}$ overexpression (N = 4 independent experiments).

(D) Summary figure illustrating role of AMPK/p27^{Kip1} signaling on autophagy, proliferation, senescence, and apoptosis.

* Signifies difference from untreated geriatric control cells; † signifies difference from AICAR-treated geriatric cells; # signifies difference from young cells; ^ signifies difference from untreated geriatric control cells ($p < 0.05$). Scale bars, 5 μm. Data are presented as means ± SE.

colony (Jackson Laboratory) and NIA rodent colony. All animal care followed the guidelines and was approved by the Institutional Animal Care and Use Committees at the Duke Medical Center.

Lentivirus Infection

Lentivirus for GFP, sh-Atg5 and scrambled sh were purchased from Dharmacon (GE Lifesciences) with titer 10^8 transduction units (TU)/mL. Lentivirus for WT p27^{Kip1} and p27^{Kip1} mutant vectors, originally described in Liang et al. (2007) were cloned and amplified at the Duke Viral Vector Core with titer 10^9 TU/mL. For *in vitro* experiments lentivirus would be added shortly after plating and left overnight before replaced with fresh media.

Senescence-Associated β-Gal Activity

Senescence-associated (SA) β-gal activity was detected in MuSCs using the senescence β-Galactosidase Staining Kit (Cell Signaling

Technology), according to manufacturer's instructions. SA β-gal$^+$ cells were quantified as percentage of the total number of cells analyzed.

Isolation of Muscle Satellite Cells

Satellite cells were isolated by methods described previously (Bareja et al., 2014). In brief, dissected muscle was digested in gentleMACS C tubes (Miltenyi Biotec). subjected to dissociation using a GentleMACS dissociator (Miltenyi Biotec). After digestion, samples were filtered, spun, re-suspended, and transferred to a 5-mL fluorescence-activated cell sorting (FACS) tube for staining. Cells were stained with the following monoclonal antibodies—CD11b (1:100), CD31 (1:100), CD45 (1:100), Ter119, and Sca1 (all conjugated to APC, eBioscience), CD34 (1:50), phycoerythrin (BD Biosciences), and ITGA7 (FITC, R&D Scientific). Following a 45-min-long incubation on ice, the cell suspension was spun down and incubated with anti-APC magnetic beads (1:10, Miltenyi Biotec) for 15 min on ice. All cells bound to APC-conjugated antibodies were separated from the original suspension using the manual MACS cell separation protocol (Miltenyi Biotec). Mouse skeletal muscle precursors were isolated by FACS using CD34 and ITGA7 as positive selection markers while CD31, CD45, CD11b, SCA1, and Ter119 were used as negative selection markers (for further details, see Supplemental Experimental Procedures).

Protein and mRNA Expression

RNA isolation, cDNA synthesis and mRNA expression was performed as described previously (White et al., 2014). Primer sequences are as follows: p21cip1 F- CCTGGTGATGTCCGACCTG, R- CCATGAGCGCATCGCAATC, p16INK4a F- CGCAGGTTCTTGGTCACTGT, R- TGTTCACGAAAGCCAGAGCG. Atg5 F- TGTGCTTCGAGATGTGTGGTT, R- ACCAACGTCAAATAGCTGACTC. Protein isolation and western blotting was performed as described previously (White et al., 2012). Primary antibodies were as follows; tubulin, PARP, AMPK, p AMPK (Thr172), S6, pS6 (Ser240/244), LC3B (Cell Signaling Technologies), p27^{Kip1} (BD Biosciences), p p27^{Kip1} (thr198) (Thermo Fisher Scientific), Histone H1 (Santa Cruz) (see Table S1).

In Vitro Immunofluorescence and Quantification

MuSCs were fixed with 4% paraformaldehyde for 15 min, washed with PBS and permeabilized with TBS-T (0.1% Triton X- [pH 8.0] TBS) for another 15 min. The cells were then blocked in 2% normal goat serum for 20 min. This was followed by incubation with respective antibodies diluted in blocking solution for 1 hr. An Alexa Fluor 488 secondary antibody (Invitrogen, cat. no. A-21121) was used for detection. The cells were counterstained with DAPI (Cell Signaling, cat. no. 4083) and Phalloidin (Cell Signaling Technology, cat. no. 8953) to visualize nuclei and actin, respectively. Images were taken using fluorescent microscopes (Zeiss). Total cell number and the percentage of cells expressing a particular fluorophore were quantified using the automated Cellomics ArrayScan. ImageJ/FIJI was used to measure densitometry for cytoplasmic/nuclear localization and quantification of cell size.

Muscle Injury

Skeletal muscle injury was performed by injection of barium chloride ($BaCl_2$) into the tibialis anterior (TA) muscle as described previously (White et al., 2009). Thirty microliters of 1.2% $BaCl_2$ (Sigma) was injected into the TA muscle.

Proliferation Assay

Quantification of cell proliferation was assayed with Click-iT EdU Alexa Fluor 594 Imaging Kit (Thermo Fisher Scientific) according to manufacturer's instructions. Quantification of EdU-positive cells was performed on the automated Cellomics ArrayScan.

Cell Apoptosis

Quantification of cellular apoptosis was assayed with TUNEL and Annexin V/PI staining. TUNEL Click-iT Plus TUNEL Assay for In Situ Apoptosis Detection, Alexa Fluor 488 dye according to manufacturer's instructions. Quantification of TUNEL-positive cells was performed on the automated Cellomics ArrayScan.

Satellite Cell Engraftment

Transplantation methods were performed as described previously (Garcia-Prat et al., 2016a; Sousa-Victor et al., 2014). In brief, FACS isolated satellite cells from young or geriatric C57BL/6 mice were plated and treated with AICAR and/or infected with the respective lentivirus overnight. The next day the media was briefly replaced and cells were collected, re-suspended in 20% fetal bovine serum F10 medium and injected into muscles previously injured with $BaCl_2$ the day before. Recipient mice were young (10–12 weeks) SCID mice. For each mouse, 10,000 cells were injected into the TA muscle. Transplantation experiments were analyzed 4 or 28 days post transplantation.

In Vivo Muscle Immunofluorescence

Immediately post dissection the whole muscle was incubated in 20% sucrose (w/v) for 12 hr then cut at the mid-belly and placed in OCT for later use. Sections (12 μm) were cut on a cryostat and dried at room temperature for 10 min. Sections were then blocked for 0.5 hr with 10% goat serum, followed by a 2-hr incubation with an anti-GFP antibody conjugated with Alex Flour 488 (Thermo Fisher Scientific, A-21311). After staining, slides were washed with PBS and mounted with mounting medium containing DAPI (Vector Laboratories, cat. no. H-1200). For quantification, six images (20×) were taken per TA muscle and GFP(+) cells or myofibers were counted and totaled for each muscle.

Cell Culture Reagents

To quantify LC3B flux MuSCs were treated with 10 μM chloroquine (Sigma) for 12 hr. To inhibit AMPK activity MuSCs were treated with 10 μM compound C (Sigma) throughout time in culture. To induce AMPK activity MuSCs were treated with 250 μM AICAR (Sigma) for the duration of time in culture. For transplantation experiments, MuSCs were treated with AICAR overnight, typically during lentiviral infection and transplanted the following day.

Cell Fractionation

Cytosolic and nuclear fractionation was performed with NE-PER Nuclear and Cytoplasmic Extraction Reagent (Thermo Scientific, no. 78833) according to manufacturer's instructions.

Approximately 1 × 10^5 cells were plated for each sample to adequately quantify protein expression in nuclear and cytoplasmic compartments.

Statistical Analysis

Data were analyzed by one-way ANOVA using Tukey's *post-hoc* analysis or two-tailed Student's t test. All data are reported as means ± SEM. Statistical analysis was performed using GraphPad Prism 6 software.

SUPPLEMENTAL INFORMATION

Supplemental Information includes Supplemental Experimental Procedures, six figures, and one table and can be found with this article online at https://doi.org/10.1016/j.stemcr.2018.06.014.

AUTHOR CONTRIBUTIONS

J.W. conceived, designed, and executed the experiments. A.B., W.K., K.H., and A.R. conceived and designed the experiments. J.W., A.B., W.K., and K.H. wrote the manuscript. M.C. executed experiments.

ACKNOWLEDGMENTS

The authors gratefully acknowledge the Duke's Cancer Center Flow Cytometry, Functional Genomics and Viral Vector Cores, for support on this project. J.P.W. was supported by funds from GlaxoSmithKline, Duke Aging Center/Pepper Center grant P30 (AG028716) and K01 (AG056664).

Received: October 10, 2017
Revised: June 19, 2018
Accepted: June 20, 2018
Published: July 19, 2018

REFERENCES

Bareja, A., Holt, J.A., Luo, G., Chang, C., Lin, J., Hinken, A.C., Freudenberg, J.M., Kraus, W.E., Evans, W.J., and Billin, A.N. (2014). Human and mouse skeletal muscle stem cells: convergent and divergent mechanisms of myogenesis. PLoS One *9*, e90398.

Blau, H.M., Cosgrove, B.D., and Ho, A.T. (2015). The central role of muscle stem cells in regenerative failure with aging. Nat. Med. *21*, 854–862.

Brooks, N.E., Schuenke, M.D., and Hikida, R.S. (2009). No change in skeletal muscle satellite cells in young and aging rat soleus muscle. J. Physiol. Sci. *59*, 465–471.

Carrano, A.C., Eytan, E., Hershko, A., and Pagano, M. (1999). SKP2 is required for ubiquitin-mediated degradation of the CDK inhibitor p27. Nat. Cell Biol. *1*, 193–199.

Cerletti, M., Jang, Y.C., Finley, L.W., Haigis, M.C., and Wagers, A.J. (2012). Short-term calorie restriction enhances skeletal muscle stem cell function. Cell Stem Cell *10*, 515–519.

Chakkalakal, J.V., Christensen, J., Xiang, W., Tierney, M.T., Boscolo, F.S., Sacco, A., and Brack, A.S. (2014). Early forming label-retaining muscle stem cells require p27kip1 for maintenance of the primitive state. Development *141*, 1649–1659.

Chakkalakal, J.V., Jones, K.M., Basson, M.A., and Brack, A.S. (2012). The aged niche disrupts muscle stem cell quiescence. Nature *490*, 355–360.

Chung, K.M., and Yu, S.W. (2013). Interplay between autophagy and programmed cell death in mammalian neural stem cells. BMB Rep. *46*, 383–390.

Collins, C.A., Zammit, P.S., Ruiz, A.P., Morgan, J.E., and Partridge, T.A. (2007). A population of myogenic stem cells that survives skeletal muscle aging. Stem Cells *25*, 885–894.

Conboy, I.M., Conboy, M.J., Wagers, A.J., Girma, E.R., Weissman, I.L., and Rando, T.A. (2005). Rejuvenation of aged progenitor cells by exposure to a young systemic environment. Nature *433*, 760–764.

Conboy, M.J., Cerletti, M., Wagers, A.J., and Conboy, I.M. (2010). Immuno-analysis and FACS sorting of adult muscle fiber-associated stem/precursor cells. Methods Mol. Biol. *621*, 165–173.

Dimri, G.P., Lee, X., Basile, G., Acosta, M., Scott, G., Roskelley, C., Medrano, E.E., Linskens, M., Rubelj, I., Pereira-Smith, O., et al. (1995). A biomarker that identifies senescent human cells in culture and in aging skin in vivo. Proc. Natl. Acad. Sci. USA *92*, 9363–9367.

Egan, D.F., Shackelford, D.B., Mihaylova, M.M., Gelino, S., Kohnz, R.A., Mair, W., Vasquez, D.S., Joshi, A., Gwinn, D.M., Taylor, R., et al. (2011). Phosphorylation of ULK1 (hATG1) by AMP-activated protein kinase connects energy sensing to mitophagy. Science *331*, 456–461.

Fry, C.S., Lee, J.D., Mula, J., Kirby, T.J., Jackson, J.R., Liu, F., Yang, L., Mendias, C.L., Dupont-Versteegden, E.E., McCarthy, J.J., et al. (2014). Inducible depletion of satellite cells in adult, sedentary mice impairs muscle regenerative capacity without affecting sarcopenia. Nat. Med. *21*, 76–80.

Fu, X., Zhu, M.J., Dodson, M.V., and Du, M. (2015). AMP-activated protein kinase stimulates Warburg-like glycolysis and activation of satellite cells during muscle regeneration. J. Biol. Chem. *290*, 26445–26456.

Fulle, S., Sancilio, S., Mancinelli, R., Gatta, V., and Di Pietro, R. (2013). Dual role of the caspase enzymes in satellite cells from aged and young subjects. Cell Death Dis. *4*, e955.

Garami, A., Zwartkruis, F.J., Nobukuni, T., Joaquin, M., Roccio, M., Stocker, H., Kozma, S.C., Hafen, E., Bos, J.L., and Thomas, G. (2003). Insulin activation of Rheb, a mediator of mTOR/S6K/4E-BP signaling, is inhibited by TSC1 and 2. Mol. Cell *11*, 1457–1466.

Garcia-Prat, L., Martinez-Vicente, M., Perdiguero, E., Ortet, L., Rodriguez-Ubreva, J., Rebollo, E., Ruiz-Bonilla, V., Gutarra, S., Ballestar, E., Serrano, A.L., et al. (2016a). Autophagy maintains stemness by preventing senescence. Nature *529*, 37–42.

Garcia-Prat, L., Munoz-Canoves, P., and Martinez-Vicente, M. (2016b). Dysfunctional autophagy is a driver of muscle stem cell functional decline with aging. Autophagy *12*, 612–613.

Gil-Gomez, G., Berns, A., and Brady, H.J. (1998). A link between cell cycle and cell death: Bax and Bcl-2 modulate Cdk2 activation during thymocyte apoptosis. EMBO J. *17*, 7209–7218.

Gwinn, D.M., Shackelford, D.B., Egan, D.F., Mihaylova, M.M., Mery, A., Vasquez, D.S., Turk, B.E., and Shaw, R.J. (2008). AMPK

phosphorylation of raptor mediates a metabolic checkpoint. Mol. Cell *30*, 214–226.

Hara, T., Nakamura, K., Matsui, M., Yamamoto, A., Nakahara, Y., Suzuki-Migishima, R., Yokoyama, M., Mishima, K., Saito, I., Okano, H., et al. (2006). Suppression of basal autophagy in neural cells causes neurodegenerative disease in mice. Nature *441*, 885–889.

Hikida, R.S. (2011). Aging changes in satellite cells and their functions. Curr. Aging Sci. *4*, 279–297.

Hiromura, K., Pippin, J.W., Fero, M.L., Roberts, J.M., and Shankland, S.J. (1999). Modulation of apoptosis by the cyclin-dependent kinase inhibitor p27(Kip1). J. Clin. Invest. *103*, 597–604.

Hong, F., Larrea, M.D., Doughty, C., Kwiatkowski, D.J., Squillace, R., and Slingerland, J.M. (2008). mTOR-raptor binds and activates SGK1 to regulate p27 phosphorylation. Mol. Cell *30*, 701–711.

Inoki, K., Li, Y., Xu, T., and Guan, K.L. (2003a). Rheb GTPase is a direct target of TSC2 GAP activity and regulates mTOR signaling. Genes Dev. *17*, 1829–1834.

Inoki, K., Zhu, T., and Guan, K.L. (2003b). TSC2 mediates cellular energy response to control cell growth and survival. Cell *115*, 577–590.

Jang, Y.C., Sinha, M., Cerletti, M., Dall'Osso, C., and Wagers, A.J. (2011). Skeletal muscle stem cells: effects of aging and metabolism on muscle regenerative function. Cold Spring Harb. Symp. Quant. Biol. *76*, 101–111.

Jejurikar, S.S., Henkelman, E.A., Cederna, P.S., Marcelo, C.L., Urbanchek, M.G., and Kuzon, W.M., Jr. (2006). Aging increases the susceptibility of skeletal muscle derived satellite cells to apoptosis. Exp. Gerontol. *41*, 828–836.

Krajnak, K., Waugh, S., Miller, R., Baker, B., Geronilla, K., Alway, S.E., and Cutlip, R.G. (2006). Proapoptotic factor Bax is increased in satellite cells in the tibialis anterior muscles of old rats. Muscle Nerve *34*, 720–730.

Liang, J., Shao, S.H., Xu, Z.X., Hennessy, B., Ding, Z., Larrea, M., Kondo, S., Dumont, D.J., Gutterman, J.U., Walker, C.L., et al. (2007). The energy sensing LKB1-AMPK pathway regulates p27(kip1) phosphorylation mediating the decision to enter autophagy or apoptosis. Nat. Cell Biol. *9*, 218–224.

Liang, J., Zubovitz, J., Petrocelli, T., Kotchetkov, R., Connor, M.K., Han, K., Lee, J.H., Ciarallo, S., Catzavelos, C., Beniston, R., et al. (2002). PKB/Akt phosphorylates p27, impairs nuclear import of p27 and opposes p27-mediated G1 arrest. Nat. Med. *8*, 1153–1160.

Machida, S., and Booth, F.W. (2004). Increased nuclear proteins in muscle satellite cells in aged animals as compared to young growing animals. Exp. Gerontol. *39*, 1521–1525.

Merlini, L., Bonaldo, P., and Marzetti, E. (2015). Editorial: pathophysiological mechanisms of sarcopenia in aging and in muscular dystrophy: a translational approach. Front. Aging Neurosci. *7*, 153.

Mizushima, N., Yamamoto, A., Matsui, M., Yoshimori, T., and Ohsumi, Y. (2004). In vivo analysis of autophagy in response to nutrient starvation using transgenic mice expressing a fluorescent autophagosome marker. Mol. Biol. Cell *15*, 1101–1111.

Montagnoli, A., Fiore, F., Eytan, E., Carrano, A.C., Draetta, G.F., Hershko, A., and Pagano, M. (1999). Ubiquitination of p27 is regulated by Cdk-dependent phosphorylation and trimeric complex formation. Genes Dev. *13*, 1181–1189.

Moss, F.P., and Leblond, C.P. (1971). Satellite cells as the source of nuclei in muscles of growing rats. Anat. Rec. *170*, 421–435.

Motti, M.L., Califano, D., Troncone, G., De Marco, C., Migliaccio, I., Palmieri, E., Pezzullo, L., Palombini, L., Fusco, A., and Viglietto, G. (2005). Complex regulation of the cyclin-dependent kinase inhibitor p27kip1 in thyroid cancer cells by the PI3K/AKT pathway: regulation of p27kip1 expression and localization. Am. J. Pathol. *166*, 737–749.

Pagano, M., Tam, S.W., Theodoras, A.M., Beer-Romero, P., Del Sal, G., Chau, V., Yew, P.R., Draetta, G.F., and Rolfe, M. (1995). Role of the ubiquitin-proteasome pathway in regulating abundance of the cyclin-dependent kinase inhibitor p27. Science *269*, 682–685.

Rathbone, C.R., Booth, F.W., and Lees, S.J. (2008). FoxO3a preferentially induces p27Kip1 expression while impairing muscle precursor cell-cycle progression. Muscle Nerve *37*, 84–89.

Ravanan, P., Srikumar, I.F., and Talwar, P. (2017). Autophagy: the spotlight for cellular stress responses. Life Sci. *188*, 53–67.

Rodgers, J.T., King, K.Y., Brett, J.O., Cromie, M.J., Charville, G.W., Maguire, K.K., Brunson, C., Mastey, N., Liu, L., Tsai, C.R., et al. (2014). mTORC1 controls the adaptive transition of quiescent stem cells from G0 to G(Alert). Nature *510*, 393–396.

Salminen, A., and Kaarniranta, K. (2012). AMP-activated protein kinase (AMPK) controls the aging process via an integrated signaling network. Ageing Res. Rev. *11*, 230–241.

Sanli, T., Steinberg, G.R., Singh, G., and Tsakiridis, T. (2014). AMP-activated protein kinase (AMPK) beyond metabolism: a novel genomic stress sensor participating in the DNA damage response pathway. Cancer Biol. Ther. *15*, 156–169.

Shefer, G., Rauner, G., Yablonka-Reuveni, Z., and Benayahu, D. (2010). Reduced satellite cell numbers and myogenic capacity in aging can be alleviated by endurance exercise. PLoS One *5*, e13307.

Sinha, M., Jang, Y.C., Oh, J., Khong, D., Wu, E.Y., Manohar, R., Miller, C., Regalado, S.G., Loffredo, F.S., Pancoast, J.R., et al. (2014). Restoring systemic GDF11 levels reverses age-related dysfunction in mouse skeletal muscle. Science *344*, 649–652.

Sousa-Victor, P., Gutarra, S., Garcia-Prat, L., Rodriguez-Ubreva, J., Ortet, L., Ruiz-Bonilla, V., Jardi, M., Ballestar, E., Gonzalez, S., Serrano, A.L., et al. (2014). Geriatric muscle stem cells switch reversible quiescence into senescence. Nature *506*, 316–321.

Sousa-Victor, P., and Munoz-Canoves, P. (2016). Regenerative decline of stem cells in sarcopenia. Mol. Aspects Med. *50*, 109–117.

Sun, X., Momen, A., Wu, J., Noyan, H., Li, R., von Harsdorf, R., and Husain, M. (2014). p27 protein protects metabolically stressed cardiomyocytes from apoptosis by promoting autophagy. J. Biol. Chem. *289*, 16924–16935.

Tang, A.H., and Rando, T.A. (2014). Induction of autophagy supports the bioenergetic demands of quiescent muscle stem cell activation. EMBO J. *33*, 2782–2797.

Tee, A.R., Manning, B.D., Roux, P.P., Cantley, L.C., and Blenis, J. (2003). Tuberous sclerosis complex gene products, Tuberin and Hamartin, control mTOR signaling by acting as a GTPase-

activating protein complex toward Rheb. Curr. Biol. *13*, 1259–1268.

Theret, M., Gsaier, L., Schaffer, B., Juban, G., Ben Larbi, S., Weiss-Gayet, M., Bultot, L., Collodet, C., Foretz, M., Desplanches, D., et al. (2017). AMPKalpha1-LDH pathway regulates muscle stem cell self-renewal by controlling metabolic homeostasis. EMBO J. *36*, 1946–1962.

von Maltzahn, J., Jones, A.E., Parks, R.J., and Rudnicki, M.A. (2013). Pax7 is critical for the normal function of satellite cells in adult skeletal muscle. Proc. Natl. Acad. Sci. USA *110*, 16474–16479.

White, J.P., Baltgalvis, K.A., Sato, S., Wilson, L.B., and Carson, J.A. (2009). Effect of nandrolone decanoate administration on recovery from bupivacaine-induced muscle injury. J. Appl. Physiol. *107*, 1420–1430.

White, J.P., Gao, S., Puppa, M.J., Sato, S., Welle, S.L., and Carson, J.A. (2012). Testosterone regulation of Akt/mTORC1/FoxO3a signaling in skeletal muscle. Mol. Cell Endocrinol. *365*, 174–186.

White, J.P., Wrann, C.D., Rao, R.R., Nair, S.K., Jedrychowski, M.P., You, J.S., Martinez-Redondo, V., Gygi, S.P., Ruas, J.L., Hornberger, T.A., et al. (2014). G protein-coupled receptor 56 regulates mechanical overload-induced muscle hypertrophy. Proc. Natl. Acad. Sci. USA *111*, 15756–15761.

Wu, F.Y., Wang, S.E., Sanders, M.E., Shin, I., Rojo, F., Baselga, J., and Arteaga, C.L. (2006). Reduction of cytosolic p27(Kip1) inhibits cancer cell motility, survival, and tumorigenicity. Cancer Res. *66*, 2162–2172.

Zhang, Y., Gao, X., Saucedo, L.J., Ru, B., Edgar, B.A., and Pan, D. (2003). Rheb is a direct target of the tuberous sclerosis tumour suppressor proteins. Nat. Cell Biol. *5*, 578–581.

Stem Cell Reports, Volume *11*

Supplemental Information

The AMPK/p27^{Kip1} Axis Regulates Autophagy/Apoptosis Decisions in Aged Skeletal Muscle Stem Cells

James P. White, Andrew N. Billin, Milton E. Campbell, Alan J. Russell, Kim M. Huffman, and William E. Kraus

Figure S1

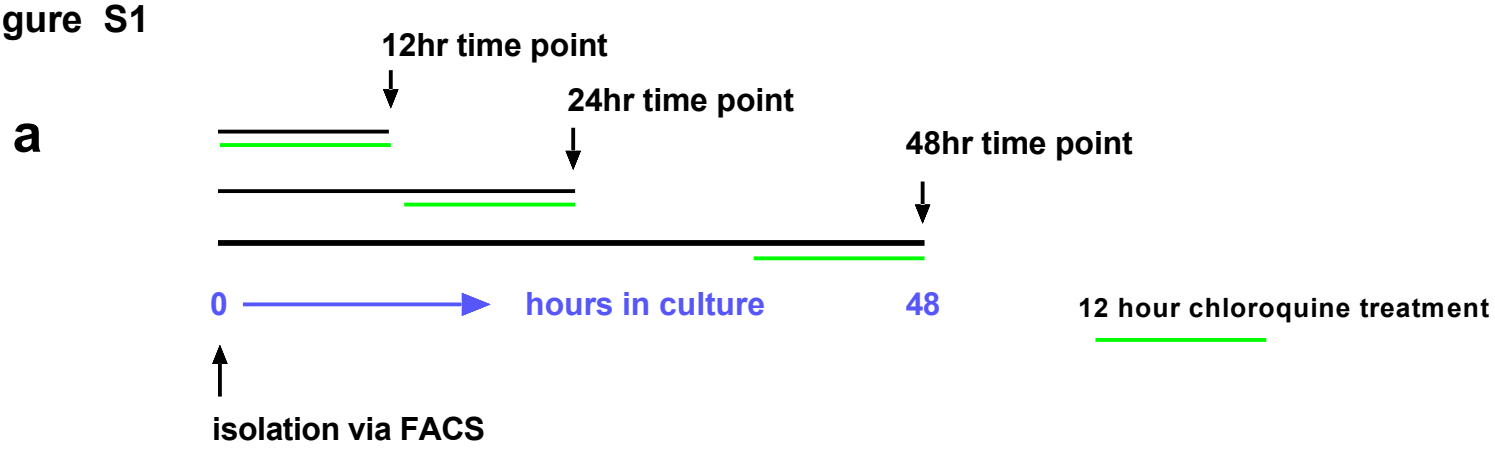
a
12hr time point
24hr time point
48hr time point
0
hours in culture
48
12 hour chloroquine treatment
isolation via FACS

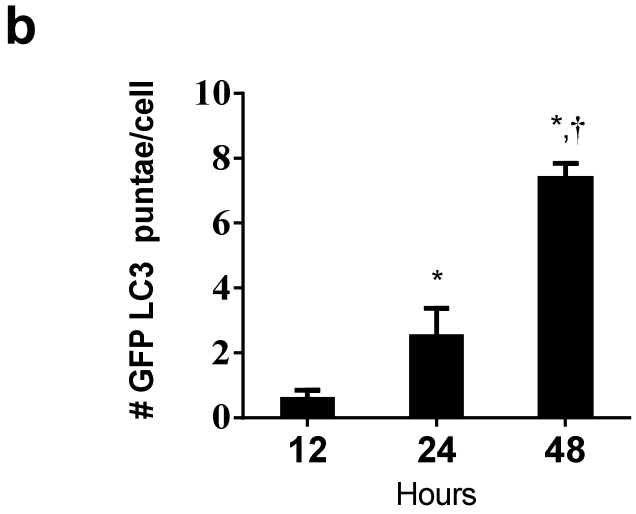
b
GFP LC3 puntae/cell
10
8
6
4
2
0
*
*,†
12
24
48
Hours

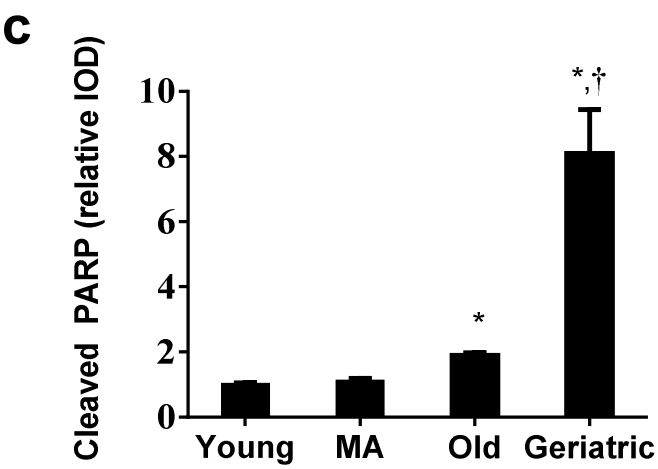
c
Cleaved PARP (relative IOD)
10
8
6
4
2
0
*
*,†
Young
MA
Old
Geriatric

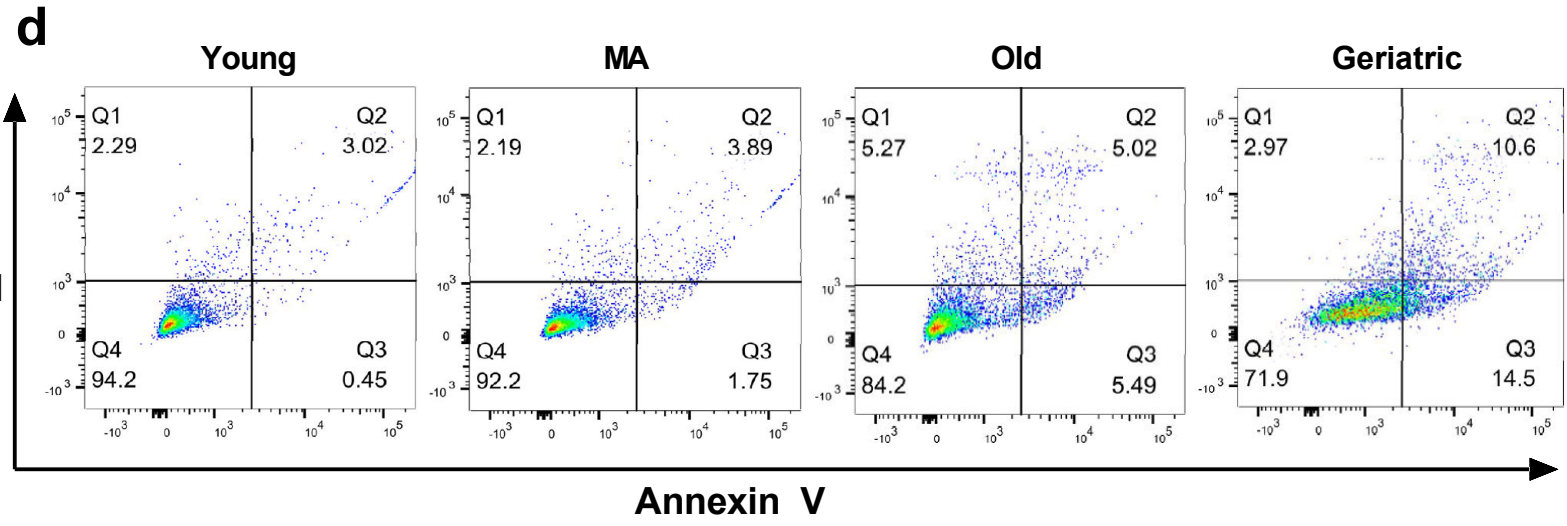
d
Young
MA
Old
Geriatric
PI
Annexin V
Q1 2.29
Q2 3.02
Q4 94.2
Q3 0.45
Q1 2.19
Q2 3.89
Q4 92.2
Q3 1.75
Q1 5.27
Q2 5.02
Q4 84.2
Q3 5.49
Q1 2.97
Q2 10.6
Q4 71.9
Q3 14.5

Figure S2

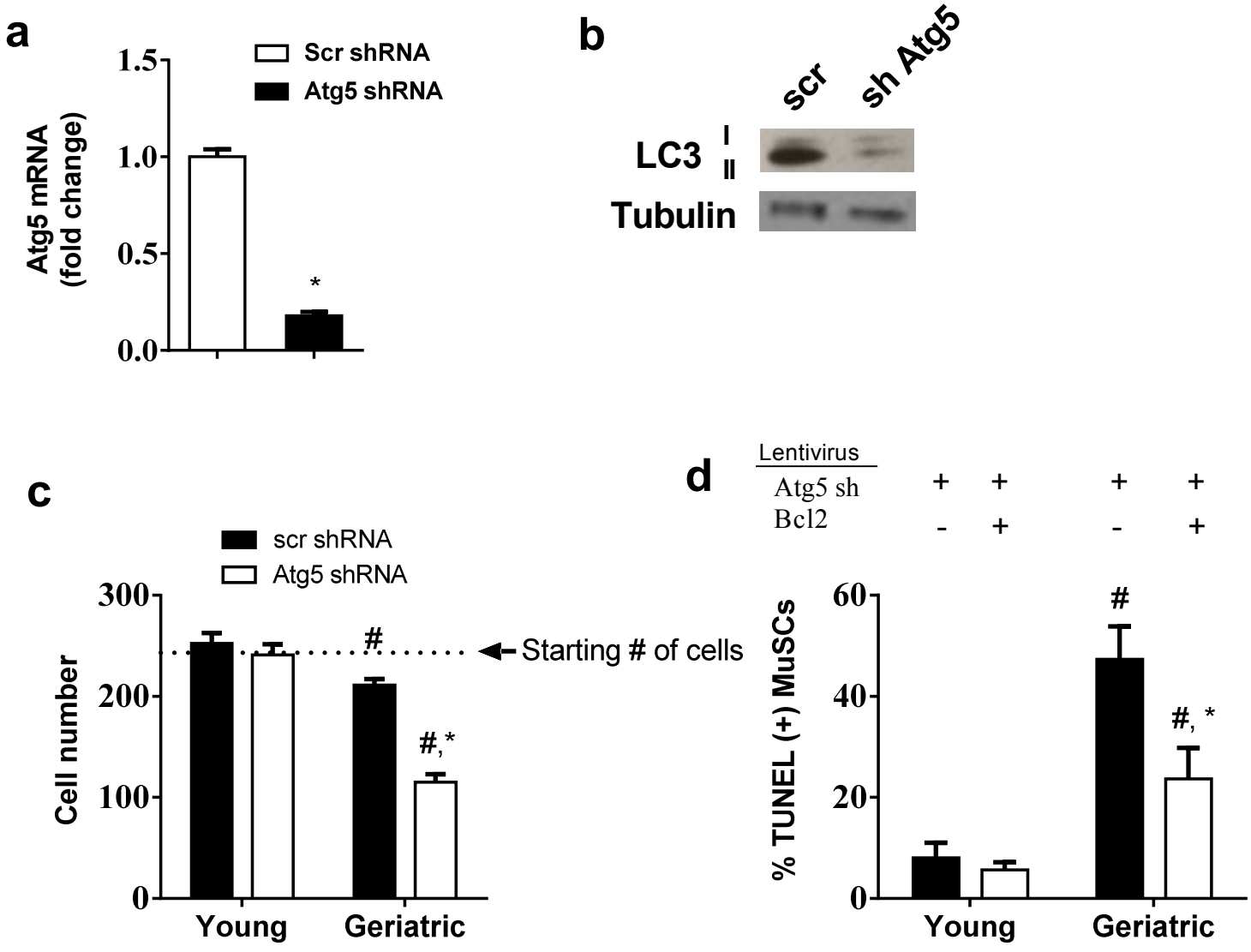
a
Scr shRNA
Atg5 shRNA
Atg5 mRNA (fold change)
1.5
1.0
0.5
0.0
*
b
scr
sh Atg5
LC3 I
II
Tubulin
c
scr shRNA
Atg5 shRNA
Cell number
300
200
100
0
#
#,*
Starting # of cells
Young
Geriatric
d
Lentivirus
Atg5 sh + + + +
Bcl2 - + - +
% TUNEL (+) MuSCs
60
40
20
0
#
#, *
Young
Geriatric

Figure S3

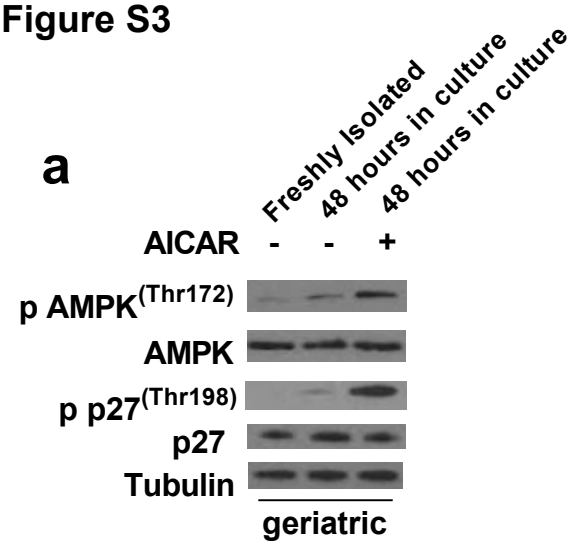
a
Freshly Isolated
48 hours in culture
48 hours in culture
AICAR - - +
p AMPK(Thr172)
AMPK
p p27(Thr198)
p27
Tubulin
geriatric

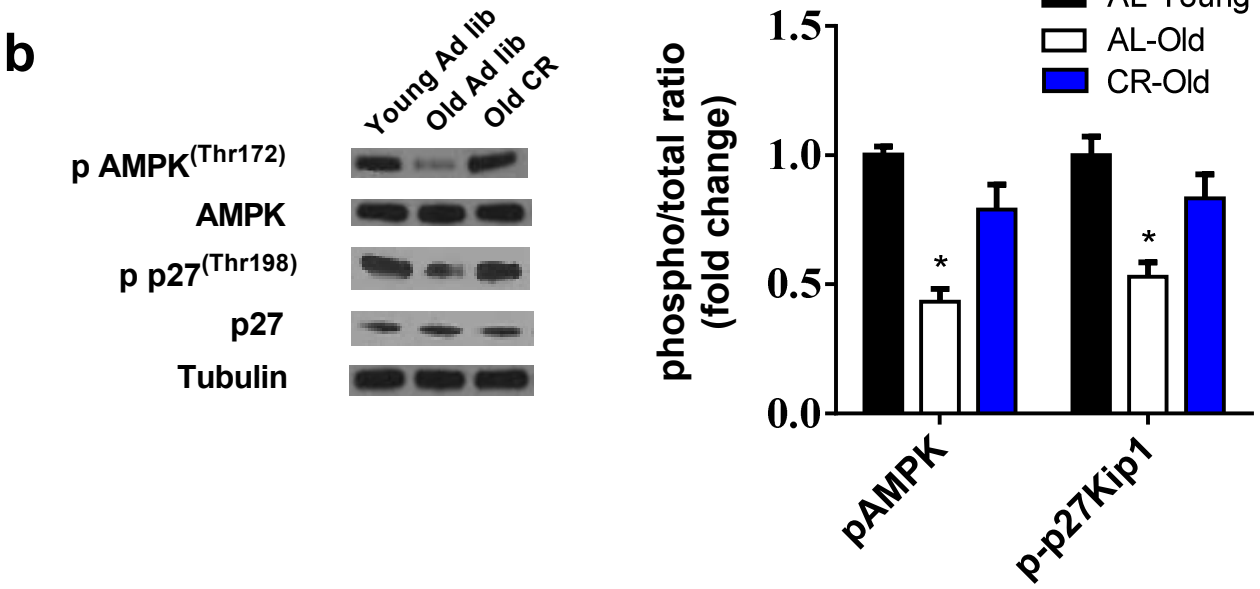
b
Young Ad lib
Old Ad lib
Old CR
p AMPK(Thr172)
AMPK
p p27(Thr198)
p27
Tubulin
AL-Young
AL-Old
CR-Old
phospho/total ratio (fold change)
1.5
1.0
0.5
0.0
*
*
pAMPK
p-p27Kip1

Figure S4

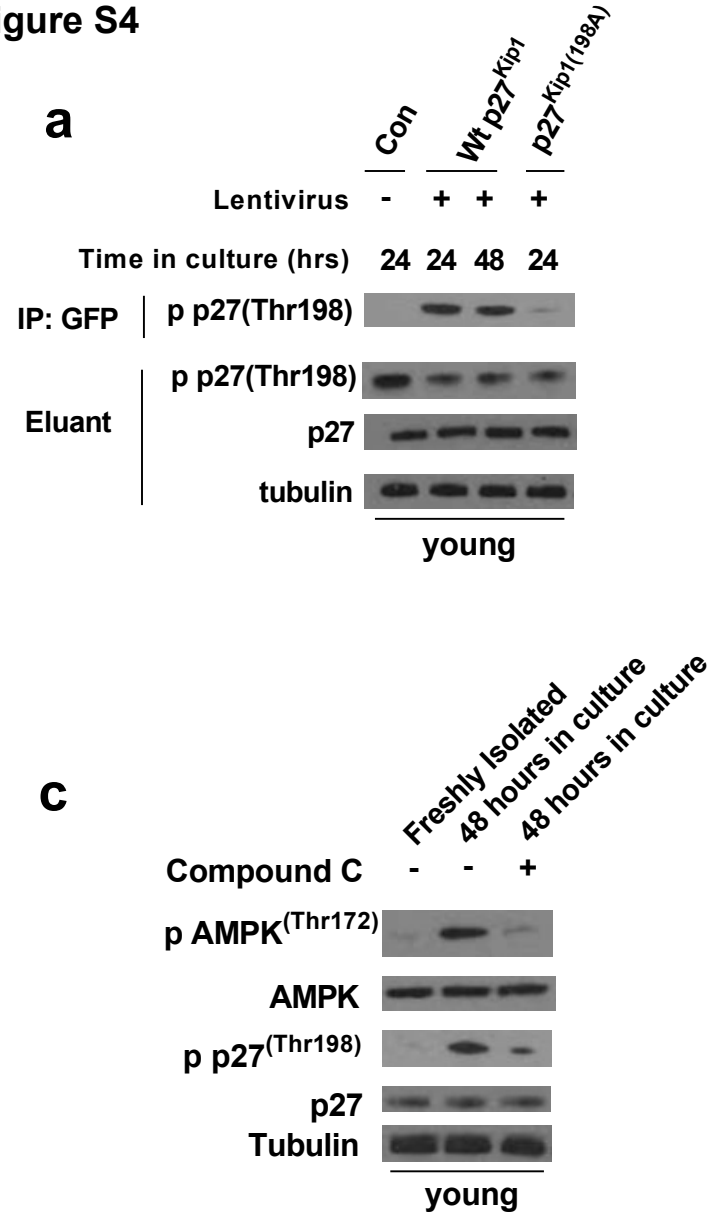
a
Con
Wt p27Kip1
p27Kip1(198A)
Lentivirus - + + +
Time in culture (hrs) 24 24 48 24
IP: GFP
p p27(Thr198)
Eluant
p p27(Thr198)
p27
tubulin
young

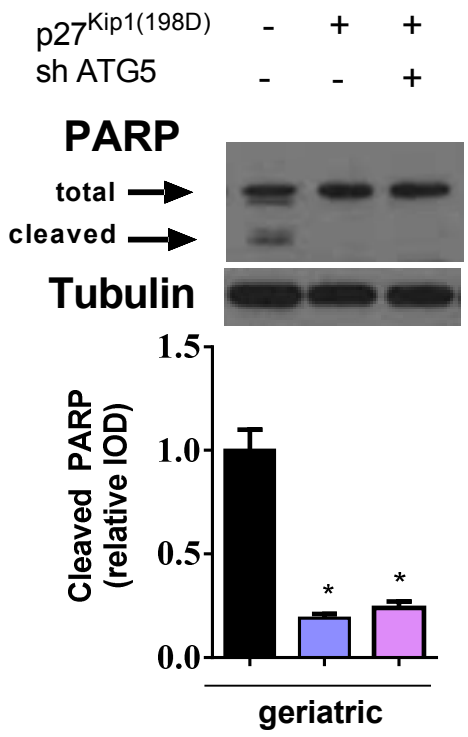
b
p27Kip1(198D) - + +
sh ATG5 - - +
PARP
total
cleaved
Tubulin
Cleaved PARP (relative IOD)
1.5
1.0
0.5
0.0
*
*
geriatric

c
Freshly Isolated
48 hours in culture
48 hours in culture
Compound C - - +
p AMPK(Thr172)
AMPK
p p27(Thr198)
p27
Tubulin
young

Figure S5

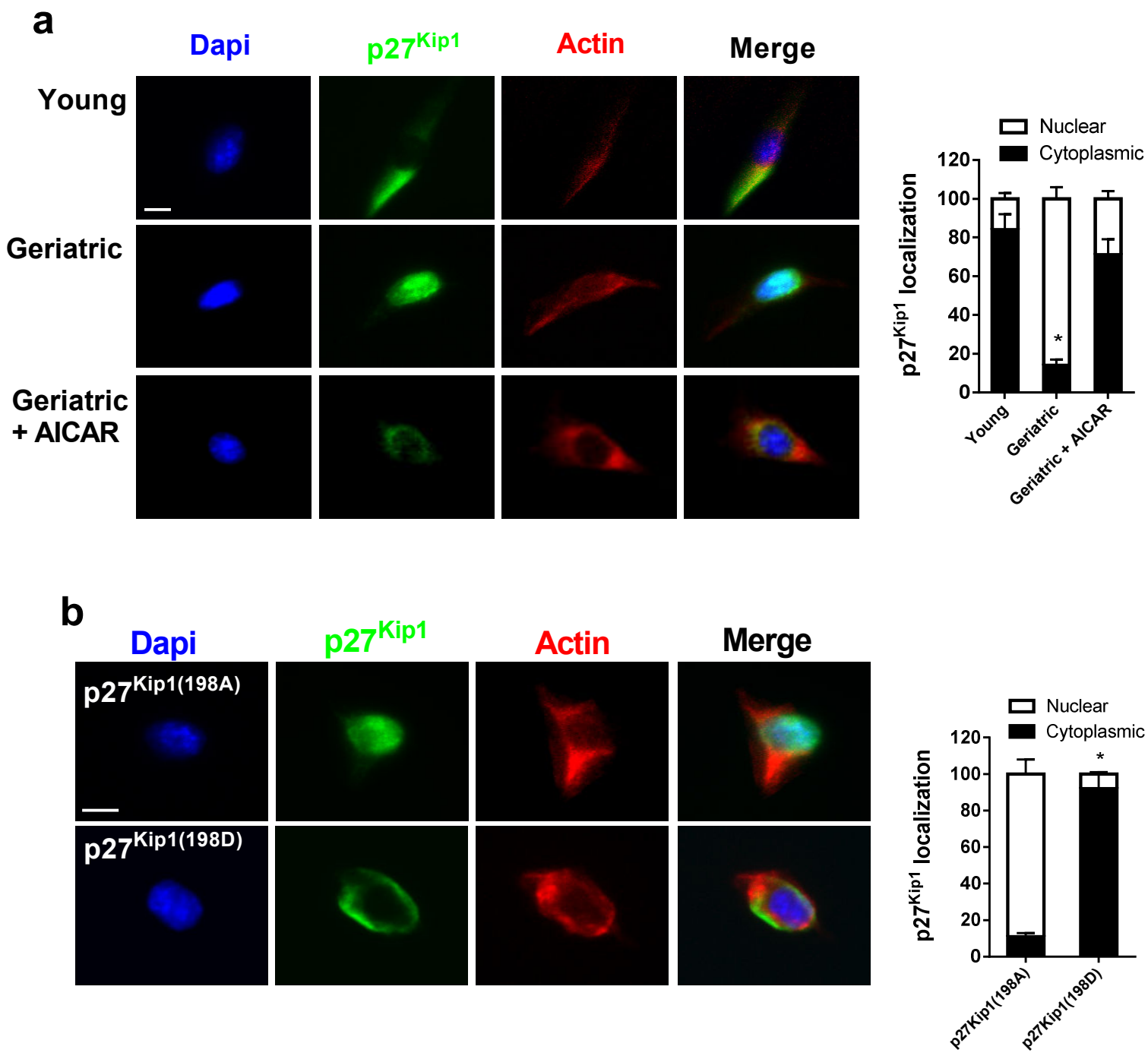
a
Dapi
p27Kip1
Actin
Merge
Young
Geriatric
Geriatric + AICAR
Nuclear
Cytoplasmic
p27Kip1 localization
120
100
80
60
40
20
0
*
Young
Geriatric
Geriatric + AICAR
b
Dapi
p27Kip1
Actin
Merge
p27Kip1(198A)
p27Kip1(198D)
Nuclear
Cytoplasmic
p27Kip1 localization
120
100
80
60
40
20
0
*
p27Kip1(198A)
p27Kip1(198D)

Figure S6

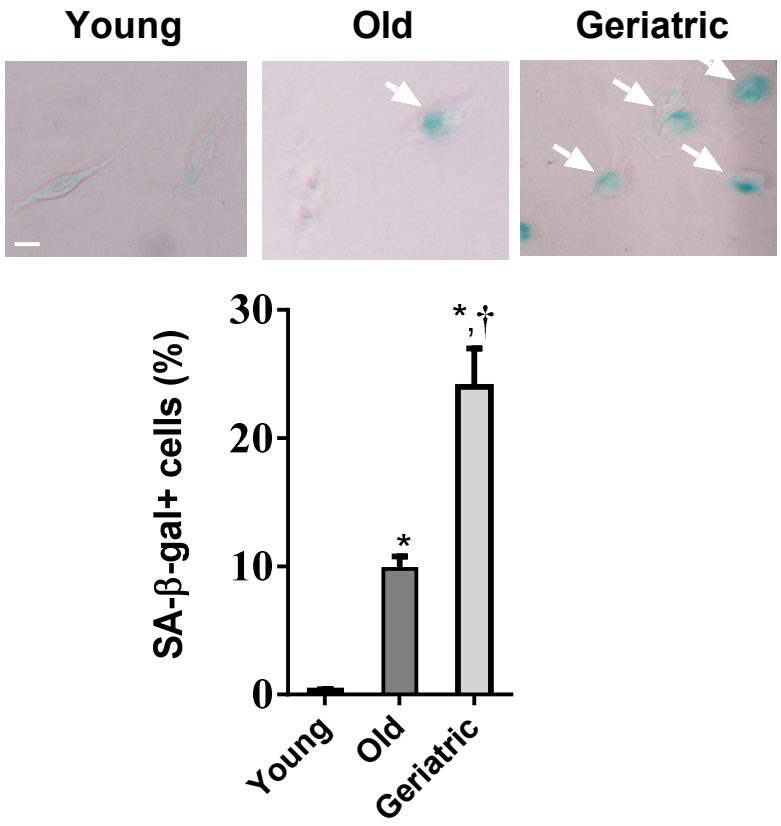
Young
Old
Geriatric
SA-β-gal+ cells (%)
30
20
10
0
*
*,†
Young
Old
Geriatric

FIGURE LEGENDS

Figure S1, related to Figure 1. Autophagy in the MuSC increases through 48 hours in culture. A. Experimental design for quantification of young MuSC LC3B punta at 12, 24 and 48 hours in culture. All cells were treated with chloroquine for 12 hours prior to collection. B. Average number of LC3B puncta per MuSC throughout the 48-hour culture time course. (N=3 independent experiments) C. Quantified cleaved PARP expression (corresponding to Figure 1C). (N=4 independent experiments) D. Annexin V x PI FACS plots of young, middle-aged, old and geriatric MuSCs after 48 hours in culture. 6.5K cells were recorded per group. * signifies difference from 12 hours. † signifies difference from 24 hour time point. ($p<0.05$). Data are presented as mean ± SE.

Figure S2, related to Figure 2. Atg5 knockdown reduces autophagy and induces cell death in the MuSC

A. Relative mRNA expression of Atg5 in young MuSCs infected with lentivirus containing scrambled sh or sh to Atg5. (N=3 independent experiments) B. LC3B isoform protein expression with over-expression of scrambled sh or sh to Atg5. C. MuSC cell number after 48 hours in culture with or without Atg5 knockdown. All groups were initially plated with 250 freshly sorted cells. (N=4 independent experiments) D. TUNEL staining in young and geriatric MuSCs during Atg5 knockdown with or without Bcl2 over-expression. (N=3 independent experiments). # signifies difference from treatment-matched cells. * signifies difference from age-matched treatment or control group. ($p<0.05$). Data are presented as mean ± SE.

Figure S3, related to Figure 3. *AMPK modulators and caloric restriction regulate AMPK/*p27^{Kip1} signaling in the MuSC. A. Representative western blots of phosphorylated and total AMPK and p27^{Kip1} in geriatric MuSCs treated with AICAR for the last 24 hours in culture (48 hours total time in culture). B *left,* representative western blots of phosphorylated and total

AMPK and p27^{Kip1} in young and old MuSCs sorted from mice fed ad libitum (AL) or under caloric restriction (CR) for 3 months. MuSCs were cultured for 48 hours. *Right*, quantified relative protein expression of phospho/total protein ratio of the indicated protein. (N=4 independent experiments). * signifies difference from ad libitum young mice. ($p<0.05$). Data are presented as mean ± SE.

Figure S4, related to Figure 4. Genetic and pharmacological methods for AMPK and p27^{Kip1} loss of function. A. AMPK-specific phosphorylation is suppressed during forced expression of the p27$^{Kip1(198A)}$ mutant. GFP pulldown assay to isolate exogenous p27^{Kip1} shows a reduced phosphorylation at Thr198 at 24 hours in culture. The reduction in phospho status was not observed with forced expression of wild-type exogenous p27^{Kip1}. B. *upper*, total and cleaved PARP protein expression in geriatric MuSCs during over-expression of p27$^{Kip1(198D)}$ and an sh to Atg5. *lower*, quantification of cleaved PARP in the respective treatment groups. (N=3 independent experiments) C. Treatment of AMPK inhibitor compound C on young MuSCs suppresses phosphorylation of AMPK and p27^{Kip1}. * signifies difference from untreated control MuSCs. ($p<0.05$). Data are presented as mean ± SE.

Figure S5, related to Figure 5. Age and genetic alteration of p27^{Kip1} phosphorylation activity is associated with p27^{Kip1} cellular location. A. *left,* IF p27^{Kip1} expression in young control and geriatric MuSCs with or without AICAR treatment. *right*, Quantification of p27^{Kip1} cellular location in all groups. (N=3 independent experiments) B. *left*, IF p27^{Kip1} expression in young MuSCs over-expressing p27$^{Kip1(198A)}$ or p27$^{Kip1(198D)}$. *right*, Quantification of p27^{Kip1} cellular location in both treatment groups. (N=3 independent experiments). Blue, DAPI, green, p27^{Kip1}, red, actin. Scale bar, 5μm. * signifies difference from young or p27$^{Kip1(198A)}$ over-expressing MuSCs. ($p<0.05$). Data are presented as mean ± SE.

Figure S6, related to Figure 6. Age-related induction of senescence. *Upper***,** β Gal positive staining in young, old and geriatric MuSCs in culture for 48 hours. *Lower*, Quantification of percentage β Gal positive cells across age groups. (N=3 independent experiments). * signifies difference from young cells. † signifies difference from old cells. ($p<0.05$). Scale bars, 5μm. Data are presented as mean ± SE.

Supplemental Experimental Procedures

Animals. C57BL/6J (Wild-type, Wt) mice were used at 3-4, 12, 24, or >28 months of age. All aged mice were obtained from the GSK aging colony (Jackson labs) and NIA rodent colony. All animal care followed the guidelines and was approved by the Institutional Animal Care and Use Committees (IACUCs) at Duke Medical Center.

Lentivirus infection. Lentivirus for GFP, sh-Atg5 and scrambled sh were purchased from Dharmacon (GE Lifesciences) with titer 10^8 TU/ml. Lentivirus for wild-type $p27^{Kip1}$ and $p27^{Kip1}$ mutant vectors, originally described in Liang et al (Liang et al., 2007) were cloned and amplified at the Duke Viral Vector Core with titer 10^9 TU/ml. For *in vitro* experiments LV would be added shortly after plating and left overnight before replaced with fresh media.

Isolation of muscle Satellite Cells Skeletal muscle was dissected (roughly 2 grams/mouse) and isolated by methods previously described (Bareja et al., 2014). Briefly, dissected muscle was distributed evenly to gentleMACS C tubes (Miltenyi Biotec) containing 15 ml of a collagenase-dispase solution (2.4 U ml^{-1} dispase, Gibco; 2 mg ml^{-1}, Sigma). The muscle was incubated at 37°C in a water bath for 45 minutes and subjected to dissociation using a GentleMACS dissociator (Miltenyi Biotec) every 15 minutes. 1 ml of heat-inactivated horse serum (Invitrogen, Life Technologies) was added to each tube to halt the digestion reaction. All solutions were brought up to 30 ml by adding PBS and passed through 40 micron mesh filters (BD Bioscience), and centrifuged for 10 minutes at 1600 rpm and 4°C. The supernatant was discarded and the remaining pellet was resuspended in 2 ml of staining solution (2% heat-inactivated horse serum in HBSS), which was transferred to a 5 ml FACS tube. This solution was again centrifuged for 10 minutes at 1600 rpm and 4°C. This was repeated twice to obtain a clean pellet containing mononuclear cells. This pellet was resuspended in staining solution and stained with the following monoclonal antibodies – CD11b (1:100), CD31 (1:100), CD45 (1:100), Ter119 and Sca1 (all conjugated to APC, eBioscience), C34 (1:50), phycoerythrin (PE), (BD

Bioscience) and ITGA7 (FITC, R&D Scientific). Following a 45 minute-long incubation on ice, the cell suspension was washed with staining solution and centrifuged for 10 minutes at 1600 rpm and 4°C. The resulting pellet was incubated with anti-APC magnetic beads (1:10, Miltenyi Biotec) for 15 minutes on ice. The cell suspension was then washed with staining solution and centrifuged for 10 minutes at 1600 rpm and 4°C. The resulting pellet was resuspended in staining solution and all the cells bound to APC-conjugated antibodies were separated from the original suspension using the manual MACS cell separation protocol (Miltenyi Biotec), following manufacturer's instructions. The flow-through was centrifuged for 10 minutes at 1600 rpm at 4°C. Mouse SMPs were isolated by FACS using CD34 and ITGA7 as positive selection markers while CD31, CD45, CD11b, SCA1, and Ter119 were used as negative selection markers. These cells were either processed for downstream experiments or seeded in plates coated with collagen I (1 μg ml^{-1}, BD Bioscience) and laminin (10 μg ml^{-1}, BD Bioscience) in myogenic growth media (20% heat-inactivated horse serum, 1% pencillin/streptomycin and 5 ng ml^{-1} bFGF in F10). 384 well plates were used for all IF imaging and seeded at 250 cells/well to 500 cells/well while 96 or 24 well plates were used for RNA and protein expression assays.

Senescence-associated (SA)-β-Gal activity. SA-β-Gal activity was detected in MuSCs using the senescence β-galactosidase staining kit (Cell Signaling), according to manufacturer's instructions. SA-β-gal^{+} cells were quantified as percentage of the total number of cells analyzed.

Protein and mRNA expression. RNA isolation, cDNA synthesis and mRNA expression was performed as previously described (White et al., 2014). Primer sequences are as follows: p21cip1 F- CCTGGTGATGTCCGACCTG, R- CCATGAGCGCATCGCAATC, p16INK4a F- CGCAGGTTCTTGGTCACTGT, R- TGTTCACGAAAGCCAGAGCG. F- TGTGCTTCGAGATGTGTGGTT, R- ACCAACGTCAAATAGCTGACTC. Protein isolation and western blotting was performed as previously described (White et al., 2012). Primary antibodies were as follows; tubulin (Cell Signaling Technologies, Cat# 2146S), PARP (Cell Signaling

Technologies, Cat# 9542S), AMPK (Cell Signaling Technologies, Cat# 2532), p AMPK (Thr172) (Cell Signaling Technologies, Cat# 2535), LC3B (Cell Signaling Technologies, Cat# 2775) ($p27^{Kip1}$ (BD Biosciences, Cat# 554069), p $p27^{Kip1}$ (thr198) (ThermoFisher, Cat# PA5-36862), Histone H1 (Santa Cruz, Cat# sc8030).

***In Vitro* immunofluorescence and quantification.** MuSCs were fixed with 4% paraformaldehyde for 15 minutes, washed with PBS and permeabilized with TBS-T (0.1% Triton-X in pH 8.0 TBS) for another 15 minutes. The cells were then blocked in 2% normal goat serum (NGS) for 20 minutes. This was followed by incubation with respective antibodies diluted in blocking solution for 1 hr. An Alexa Fluor 488 secondary antibody (Invitrogen, Cat# A-21121) was used for detection. The cells were counterstained with DAPI (Cell Signaling, Cat # 4083) and Phalloidin (Cell Signaling, Cat # 8953) to visualize nuclei and actin, respectively. Images were taken using fluorescent microscopes (Zeiss). Total cell number and the percentage of cells expressing a particular fluorophore were quantified using the automated Cellomics ArrayScan©. ImageJ/FIJI was used to measure densitometry for cytoplasmic/nuclear localization and quantification of cell size.

Muscle injury Skeletal muscle injury was performed by injection of barium chloride ($BaCl_2$) into the Tibialis Anterior (TA) muscle as previously described (White et al., 2009). 30µl of 1.2% $BaCl_2$ (sigma) was injected. A small (1 cm) incision was made in the skin overlying the distal 1/3 of the TA. A 25 gauge, 5/8 (0.5 x 16 mm) needle was inserted along the longitudinal axis of the muscle and the $BaCl_2$ injected slowly as the needle was withdrawn. A second injection was performed approximately 3 mm and at a 15 degree angle from the first injection. After the injection, the skin was bound with Vet-bond adhesive.

Proliferation assay Quantification of cell proliferation was assayed with Click-iT® EdU Alexa Fluor® 594 Imaging kit (ThermoFisher) according to manufacturer's instructions. Quantification of EdU Positive cells was performed on the automated Cellomics ArrayScan©.

Caloric restriction The CR protocol is based on previously published work showing CR enhanced satellite cell function in both young and old mice (Cerletti et al., 2012). All mice were fed ad lib*itum* (AL) until 2 months (young mice) or 23 months (aged mice) of age, and during this time, their baseline food intake was determined. Mice were then switched to a CR diet for the next 12 weeks (1 week at 20% restriction (80% of baseline calorie intake) and 11 weeks at 40% restriction (60% of baseline calorie intake). Control mice were maintained on a 90% diet for the entire 12 weeks. Analysis of *in vitro* muscle stem cell function was performed after 12 weeks of CR or control diet, when animals are 5 months or 24 months of age.

Cell apoptosis. Quantification of cellular apoptosis was assayed with TUNEL and Annexin V/PI staining. TUNEL Click-iT® Plus TUNEL Assay for In Situ Apoptosis Detection, Alexa Fluor® 488 dye according to manufacturer's instructions. Quantification of TUNEL Positive cells was performed on the automated Cellomics ArrayScan©. Apoptosis detection by Annexin V and propidium iodide (PI) staining (ThermoFisher) was performed according to the manufacturer's instructions. Annexin and PI(+) cells were quantified using BD FACSCanto II flow cytometer.

***In Vivo* muscle immunofluorescence** Immediately post dissection the whole muscle was incubated in 20% sucrose for 12 hours then cut at the mid-belly and placed in OCT for later use. 12µm sections were cut on a cryostat and dried at room temperature for 10 minutes. Sections were then blocked for 0.5 hour with 10% goat serum, followed by a 2hr incubation with an anti-GFP antibody conjugated with Alex Flour 488 (ThermoFisher, A-21311). After staining, slides

were washed with PBS and mounted with mounting medium containing DAPI (Vector Laboratories, Cat # H-1200). For quantification, six images (20x) were taken per TA muscle and GFP(+) cells or myofibers were counted and totaled for each muscle.

Cell Culture reagents To quantify LC3B flux MuSCs were treated with 10μM Chloroquine (Sigma) for 12 hours. To inhibit AMPK activity MuSCs were treated with 10μM Compound C (Sigma) throughout time in culture. To induce AMPK activity MuSCs were treated with 250μM 5-Aminoimidazole-4-carboxamide 1-β-D-ribofuranoside (AICAR, Sigma) for the duration of time in culture. For transplantation experiments, MuSCs were treated with AICAR overnight, typically during lentiviral infection and transplanted the following day.

Statistical Analysis Data were analyzed by One Way ANOVA using Tukey's post hoc analysis or two-tailed Student's t-test. All data are reported as mean ± SEM. Statistical analysis was performed using GraphPad Prism 6 software.

REFERENCES

Bareja, A., Holt, J.A., Luo, G., Chang, C., Lin, J., Hinken, A.C., Freudenberg, J.M., Kraus, W.E., Evans, W.J., and Billin, A.N. (2014). Human and mouse skeletal muscle stem cells: convergent and divergent mechanisms of myogenesis. PLoS One *9*, e90398.

Cerletti, M., Jang, Y.C., Finley, L.W., Haigis, M.C., and Wagers, A.J. (2012). Short-term calorie restriction enhances skeletal muscle stem cell function. Cell Stem Cell *10*, 515-519.

Liang, J., Shao, S.H., Xu, Z.X., Hennessy, B., Ding, Z., Larrea, M., Kondo, S., Dumont, D.J., Gutterman, J.U., Walker, C.L.*, et al.* (2007). The energy sensing LKB1-AMPK pathway regulates p27(kip1) phosphorylation mediating the decision to enter autophagy or apoptosis. Nat Cell Biol *9*, 218-224.

White, J.P., Baltgalvis, K.A., Sato, S., Wilson, L.B., and Carson, J.A. (2009). Effect of nandrolone decanoate administration on recovery from bupivacaine-induced muscle injury. J Appl Physiol *107*, 1420-1430.

White, J.P., Gao, S., Puppa, M.J., Sato, S., Welle, S.L., and Carson, J.A. (2012). Testosterone regulation of Akt/mTORC1/FoxO3a signaling in skeletal muscle. Mol Cell Endocrinol.

White, J.P., Wrann, C.D., Rao, R.R., Nair, S.K., Jedrychowski, M.P., You, J.S., Martinez-Redondo, V., Gygi, S.P., Ruas, J.L., Hornberger, T.A.*, et al.* (2014). G protein-coupled receptor 56 regulates mechanical overload-induced muscle hypertrophy. Proc Natl Acad Sci U S A *111*, 15756-15761.

Antibody	Use	Vendor	Catolog #
S6	WB	Cell Signaling Technologies	2217
p S6 (Ser240/244)	WB	Cell Signaling Technologies	5364
LC3B	WB/IF	Cell Signaling Technologies	2775
AMPKα	WB	Cell Signaling Technologies	2532
p AMPK (Thr172)	WB	Cell Signaling Technologies	2535
β tubulin	WB	Cell Signaling Technologies	2146
PARP	WB	Cell Signaling Technologies	9542
p27Kip1	WB/IF	BD Biosciences	554069
p p27kip1 (Thr198)	WB	ThermoFisher	PA5-36862
Histone H1	WB	Santa Cruz	sc8030
CD11b	Flow	eBioscience	17-0112-82
CD31	Flow	eBioscience	17-0311-82
CD45	Flow	eBioscience	17-0451-82
Ter119	Flow	eBioscience	17-5921-82
Sca1	Flow	eBioscience	17-5981-81
CD34	Flow	BD Biosciences	551387
ITGA7	Flow	R and D Biosystems	FAB3518F

Table 1.